~~Measurements of~~ Ozone Deposition to a Coastal Sea~~:~~ ~~by~~ Comparison of Eddy Covariance Observations with Reactive Air-Sea Exchange Models

David C. Loades[1], Mingxi Yang[2], Thomas G. Bell[2], Adam R. Vaughan[1], Ryan J. Pound[1], Stefan Metzger[3,4], James D. Lee[4,5] & Lucy J. Carpenter[1]

[1]Wolfson Atmospheric Chemistry Laboratories, Department of Chemistry, University of York, University Road, York, YO10 5DD, UK
[2]Plymouth Marine Laboratory, Prospect Place, Plymouth, PL1 3DH, UK
[3]National Ecological Observatory Network Program, Battelle, 1685 38th Street, Boulder, CO 80301, USA
[4]Department of Atmospheric and Oceanic Sciences, University of Wisconsin-Madison, 1225 West Dayton Street, Madison, WI 53706, USA
[5]National Centre for Atmospheric Science, University of York, University Road, York, YO10 5DD, UK

Correspondence to: David C. Loades (dl823@york.ac.uk)

Abstract. A fast response (10 Hz) chemiluminescence detector for ozone (O_3) was used to determine O_3 fluxes using the eddy covariance technique at the Penlee Point Atmospheric Observatory (PPAO) on the south coast of the UK during April and May 2018. The median O_3 flux was -0.132 mg m^{-2} h^{-1} (0.018 ppbv m s^{-1}) corresponding to a deposition velocity of 0.037 cm s^{-1} (interquartile range 0.017–0.065 cm s^{-1}) – similar to the higher values previously reported for open ocean flux measurements, but not as high as some other coastal results. We demonstrate that a typical single flux observation was above the 2σ limit of detection, but had considerable uncertainty. The median 2σ uncertainty of deposition velocity was 0.031 cm s^{-1} for each 20-minute period, which reduces with the square root of the sample size. Eddy covariance footprint analysis of the site indicates that the flux footprint was predominantly over water (> 96%), varying ~~slightly~~ with atmospheric stability and, to a lesser extent, the tide. At very low wind speeds when the atmosphere was typically unstable, the observed ozone deposition velocity was elevated, most likely because the footprint contracted to include a greater land contribution in these conditions. At moderate-to-high wind speeds when atmospheric stability was near-neutral, the ozone deposition velocity increased with wind speed, and showed a linear dependence with friction velocity. This observed dependence on friction velocity (and therefore also wind speed) is consistent with the ~~of comparable magnitude to~~ predictions from the one-layer model of ~~(~~Fairall et al.~~,~~ (2007), which parameterises the oceanic deposition of ozone from the fundamental conservation equation, accounting for both ocean turbulence and near-surface chemical destruction, while assuming that chemical O_3 destruction by iodide is distributed over depth. The two-layer model recently developed by Luhar et al. (2018) assumes that the destruction of ozone by iodide occurs predominantly in the first layer, and that turbulence-chemistry interaction is weak compared to transfer by turbulent mixing in the layer below. The Luhar et al. (2018) parameterisation shows no major dependence of deposition velocity on wind speed, in contrast to our observations, and underestimates the measured

deposition velocities. These results call for further investigation into the mechanisms and control of oceanic O_3 deposition.~~Deposition was also elevated at very low wind speeds, most likely because the footprint contracted to include a greater land contribution in these conditions.~~

1 Introduction

Tropospheric ozone is important due to its considerable effects on human health (Medina-Ramón et al., 2006), agricultural yields (Heck et al., 1982) and global warming (Stevenson et al., 2013). Dry deposition is a major sink of tropospheric ozone, comprising ~~around~~ as much as 25% of total loss from the troposphere (Ganzeveld et al., 2009; Lelieveld and Dentener, 2000; Pound et al., 2019). Deposition to the sea surface is the greatest source of uncertainty in global estimates of total ozone dry deposition (Hardacre et al., 2015) due to deposition occurring at a slow and highly uncertain rate, but over a vast area. ~~Despite this, there are few reported observations of ozone deposition to the sea surface.~~

Ozone deposition flux is commonly parameterised according to Eq. (1) (Pacyna, 2008):

$$F = -v_d[O_3] \quad (1)$$

where F is flux in mol cm^{-2} s^{-1}, v_d is deposition velocity in cm s^{-1}, ~~F is flux in mol cm^{-2} s^{-1},~~ and [O_3] is ozone concentration in mol cm^{-3}. In models, deposition velocity is commonly calculated using a series of resistance terms, each defining barriers to deposition in separate layers (Wesely and Hicks, 2000):

$$v_d = (R_a + R_b + R_c)^{-1} \quad (2)$$

R_a is the aerodynamic resistance, independent from the species being considered. R_b represents the resistance through the quasi-laminar thin layer of air in contact with a surface – this varies with the species' diffusivity. Lastly R_c is the surface resistance, which is typically the largest barrier to deposition for insoluble gases – roughly 95% of total resistance in the case of ozone (Chang et al., 2004; Lenschow et al., 1982).

There are few reported observations of ozone deposition to the sea surface. Early work to determine oceanic O_3 deposition velocity was either laboratory-based (Garland et al, 1980; McKay et al., 1992) or used box enclosure loss rate experiments in the field (Aldaz, 1969; Galbally and Roy, 1980). Such experiments are valuable in determining ~~ed atmospheric and~~ surface resistance (describing the affinity of a surface for absorbing a given gas) ~~values~~ for ozone deposition.~~,~~ However, these experiments ~~but do not accurately~~ are limited in their ability to represent real~~-~~world physical processes such as turbulence at the air/sea interface. More recent flux measurements have been made with the eddy covariance method, which is the best way of observing fluxes in a system without perturbing it. Eddy covariance measurements have been made from coastal towers (Gallagher et al., 2001; Whitehead et al., 2009; McVeigh et al., 2010), aircraft (Lenschow et al., 1982; Kawa and Pearson, 1989), and ships (Bariteau et al., 2010; Helmig et al., 2012). The ~~reported~~ deposition velocities ~~(v_d)~~ reported in the few eddy covariance observations over saltwater vary greatly: 0.01–0.15 cm s^{-1}, with windspeed dependencies evident in some measurements and ~~absent~~ not in~~from~~ others.

Formatted: Font: Italic
Formatted: Not Superscript/ Subscript
Formatted: Font: Italic
Formatted: Font: Not Italic
Formatted: Font: Not Italic
Formatted: Font:

The reported eddy covariance measurements use two different techniques to measure ozone at high frequency, both utilising chemiluminescent reactions of ozone. In the instruments used for tower-based measurements (Gallagher et al., 2001; McVeigh et al., 2010; Whitehead et al., 2009), ozone is reacted with a coumarin-based dye on the surface of a silica gel disk. Aircraft (Kawa and Pearson, 1989; Lenschow et al., 1982) and ship-borne (Bariteau et al., 2010; Helmig et al., 2012) instruments have instead utilised the reaction between ~~ed~~ ozone and ~~with~~ gas phase nitric oxide.

Ozone deposition to the ocean ~~is likely to~~ depends both upon physical exchange, facilitated by diffusion and turbulence, and chemical reaction at the water's surface (Chang et al., 2004; Fairall et al., 2007; Luhar et al., 2018). Iodide in sea water has been identified as a key reactant (Garland et al., 1980). ~~, and t~~There has been considerable recent progress in understanding ~~its~~ the global distribution of oceanic surface iodide (Chance et al., 2014, 2019; Macdonald et al., 2014; Sherwen et al., 2019). However, there has only been one report of the dependence of the iodide – ozone rate constant with temperature (Magi et al., 1997), and this remains a considerable uncertainty in global models. Dissolved organic material (DOM) has been suggested to be of similar importance for~~to~~ ozone deposition as iodide (Martino et al., 2012; Shaw and Carpenter, 2013), especially given its enrichment in the sea surface microlayer (SML) (Zhou and Mopper, 1997). The complex and variable composition of DOM makes assessing its global reactivity ~~towards~~ with ozone a challenge.

Early work by Garland et al. (1980) formulated a description of ozone loss to sea water based on surface properties:

$$v_{dw} = \sqrt{aD} \quad (3)$$

where a is the reactivity of iodide with ozone, D is the diffusivity of ozone in water, and v_{dw} is the waterside deposition velocity, related to surface resistance (R_c) by

$$R_c = \frac{1}{\alpha v_{dw}} \quad (4)$$

where α is the dimensionless solubility (liquid/gas) of ozone in water. This interpretation incorporates the chemical properties of the reaction, but neglects turbulent diffusion and underestimates the deposition velocity in cold water. ~~(~~Fairall et al. ~~(~~, 2007) allowed deposition velocity to vary with oceanic turbulence by considering the O_3-iodide reaction beyond the molecular sublayer, obtaining the dependence:

$$v_{dw} = \sqrt{aD}\,\frac{K_1(\xi_0)}{K_0(\xi_0)} \quad (5)$$

K_0 and K_1 are modified Bessel functions of the second kind, of order 0 and 1 respectively, and

$$\xi_0 = \frac{2}{\kappa u_{*w}}\sqrt{aD} \quad (6)$$

where κ is the von Kármán constant (~0.4) and u_{*w} is the waterside friction velocity. This is sometimes referred to as a one-layer model, due to the assumption that reactivity is uniform with depth. This one-layer approach has been reported to match observations better than a using a fixed surface resistance term, but overestimates deposition velocity by a factor of 2-3 in colder waters where the rate of reaction between ozone and iodide is slower.

An alternative, two-layer scheme is explored by ~~(~~Fairall et al.~~,~~ (2007) and expanded upon by ~~(~~Luhar et al.~~,~~ (2017). The authors consider an enhancement in reactivity in a very thin layer (reaction-diffusion sublayer) at the surface, while the water

Formatted: Font: Italic

Formatted: Font: Italic

beneath has only very minor background reactivity. In a revision of the two-layer scheme, Luhar et al. (2018) assumed turbulent transfer to be negligible compared with chemical removal of ozone within the reaction-diffusion sublayer, but with both turbulence and chemistry accounted for in the layer beneath, defining the waterside deposition velocity:

$$v_{dw} = \sqrt{aD}\left[\frac{\psi K_1(\xi_\delta)cosh(\lambda)+\psi K_0(\xi_\delta)sinh(\lambda)}{\psi K_1(\xi_\delta)sinh(\lambda)+\psi K_0(\xi_\delta)cosh(\lambda)}\right] \quad (7)$$

The terms ψ, ξ_δ and λ in Eq. (7) all vary according to the reaction-diffusion sublayer depth, δ_m:

$$\psi = \sqrt{1+\frac{\kappa u_{*w}\delta_m}{D}} \quad (8)$$

$$\xi_\delta = \sqrt{\frac{4a}{\kappa u_{*w}}}\left(\delta_m + \frac{D}{\kappa u_{*w}}\right) \quad (9)$$

$$\lambda = \delta_m\sqrt{\frac{a}{D}} \quad (10)$$

Eqs. (7-10) describe the two-layer scheme that will be discussed in this work. The method of assigning a value to δ_m is discussed by (Luhar et al., (2018), who found that a fixed depth of 3 μm was a good fit to the data of (Helmig et al., (2012). When a variable reaction-diffusion sublayer depth was considered as proportional to the reaction-diffusion length scale ($l_m = \sqrt{D/a}$), Luhar et al. (2018) found it necessary to multiply l_m by a factor of 0.7 to obtain a δ_m value that fitted reasonably with observations. Pound et al. (2019) were however able to obtain a good fit to observational data without this factor by using the oceanic iodide parameterisation of (Sherwen et al., (2019) in place of that of (Macdonald et al., (2014). Pound et al. (2019), define the reaction-diffusion layer depth according to Eq. (11).

$$\delta_m = \sqrt{\frac{D}{a}} \quad (11)$$

The dependence of deposition velocity with wind speed (or friction velocity, u_*, which scales linearly with wind speed over the ocean) within these Fairall et al. (2007) and Luhar et al. (2018) models is markedly different, and it is not clear which is a better fit to existing observations. The deposition velocity estimated by the one-layer model of (Fairall et al., (2007), increases linearly with friction velocity and compares favourably with the TexAQS06 and GOMECC07 cruises (Helmig et al., 2012). However, observations made during other cruises discussed by Helmig et al. (2012) show no dependence on friction velocity. The two-layer model of (Luhar et al., (2018) predicts almost no influence of friction velocity on deposition velocity, except at very low (< 2 m s^{-1}) wind speeds.

A bBetter characterisationed of the effects of wind speed and sea-surface composition on ozone deposition sink velocity to the oceans sea surface would significantly improve our understanding of the global tropospheric O_3 cycling budget (Ganzeveld et al., 2009; Pound et al., 2019). Here we present coastal ozone flux measurements made at Penlee Point Atmospheric Observatory (PPAO; https://www.westernchannelobservatory.org.uk/penlee/) on the southwest coast of the UK using a fast response gas phase chemiluminescence detector (CLD). Causes of natural variability Factors affecting the variation and uncertainty in the observed deposition velocity are discussed, including the effects of the changing relative contributions from sea and land within the flux footprint.

2 ~~Experimental~~Materials and methods

2.1 Measurement location

The PPAO is situated on a headland just south-west of Plymouth, UK~~, located~~ (50° 19.08' N, 4° 11.35' W). The observatory is located 11 m a.m.s.l. with an extendable mast on the roof. It lies 30–60 m away from the sea, depending on tide, with the intervening land predominantly bare rock with some grass immediately surrounding the tower. For the work presented here, the top of the tower was extended to 19 m a.m.s.l. The dominant wind directions are from the south-west, followed by the north-east (Figure 1). The focus of this work is the south-west (180–240°) wind sector, which brings in air from the Atlantic Ocean and English Channel to the site (Yang et al., 2016).

2.2 Experimental set-up

The ozone chemiluminescence detector was adapted from an Eco Physics® CLD 886 NO_x detector, working on the same principle as the instrument used by Helmig et al. (2012). A supply of excess NO is introduced to the sample, which reacts with O_3 to generate NO_2 in an excited state. The relaxation process leads to emission of a photon that is amplified and detected using a photomultiplier tube (PMT). In order to maintain a low number of dark counts, the PMT is cooled to -5°C by a Peltier cooler. Clean dry air is continuously pumped over the PMT to avoid the build-up of water (Figure 2).

Sample air was drawn from the top of the tower through ~10 m of 3/8'' PFA tubing by a vacuum pump at 13.5 L min^{-1}. This maintained a turbulent flow in the main sampling line (Reynolds number ~~=~~ ~3000). A flow of 300 mL min^{-1} was drawn from this sample manifold through 1/8'' PFA tubing and into the analyser using an internal vacuum pump (Figure 2~~ part 11~~), limited by a critical orifice~~ (part 5)~~. Before entering the analyser, the sample air was first passed through a dryer~~ (part 3)~~ consisting of 60 cm of Nafion™ tubing coiled in a container of desiccant (indicating Drierite) to reduce humidity. A three-way solenoid valve~~ (part 2)~~ allowed for a sample of indoor air passed through a charcoal filter~~ (part 1)~~ to remove O_3 to record an instrument zero. A 50 mL min^{-1} flow of 2% NO in N_2 was supplied separately to the analyser at a pressure of 4 bar through approximately 1.5 m of 1/8'' PFA tubing. The NO and O_3 were then mixed immediately before the reaction chamber (~~part 9,~~ at ~26 mbar pressure) and the resulting chemiluminescence ~~was~~ detected by the PMT.

The CLD counts were logged at 10 Hz and converted into ozone mixing ratios using the signal from a co-located, recently calibrated 2B model 205 dual beam ozone monitor. The CLD sensitivity was determined to be 240 counts s^{-1} $ppbv^{-1}$ and showed no obvious dependence on ambient humidity (Figure S1~~3~~) providing evidence for the efficacy of the dryer. Instrument dark counts were 480±40 count s^{-1}, leading to a 10 Hz signal-to-noise ratio of 33 for the average 46 ppbv O_3 measured during this work.

Three-dimensional wind data were obtained from a Gill WindMaster Pro 3D sonic anemometer at 10 Hz. Humidity, air pressure and temperature data were logged at 0.25 Hz from a Gill MetPak Pro. Vertical wind data were adjusted by +16.6% and +28.9% in magnitude for positive and negative values, respectively, in line with the corrections recommended for a

reported firmware bug in the Gill WindMaster instruments: (http://gillinstruments.com/data/manuals/KN1509_WindMaster_WBug_info.pdf).

2.3 Pre-flux processing

The eddy covariance method (EC) relies on the simultaneous measurement of vertical wind speed (w) and the relevant scalar (in this case, ozone ~~concentration~~dry mixing ratio). These values were determined at 10 Hz in order to resolve the full range of eddies responsible for vertical ozone transport. It is necessary to average data over a suitable period to reduce random noise and capture transport from large eddies, whilst avoiding too long a period such that non-turbulent transport and non-stationarity become ~~issues~~more important. An averaging time of around 30 minutes is often recommended (Foken, 2008). Previous measurements of O_3 flux have used averaging periods from 10 minutes (Helmig et al., 2012) to 1 hour (Gallagher et al., 2001), and a 20-minute period was chosen for this work. Prior to the flux calculation, data were despiked using a median filter despiking method (Brock, 1986; Starkenburg et al., 2016) using an order of N = 4 (9 points in a window). This involves binning the differences from the normalised data into exponentially more bins until bins exist within the range of the histogram that have zero values. Difference values beyond these empty bins are then identified as spikes and removed. For the flux calculation, data were linearly detrended to determine deviation from the mean within the averaging period. A double rotation was applied to the wind data in each averaging period to align the u axis with the mean wind and remove any tilt in the wind vector, resulting in a mean vertical wind of zero. A planar fit method (Wilczak~~, James~~ et al., 2001) was considered as an alternative to double rotation, but a single set of planar fit coordinates was found to be inappropriate for the Penlee site. Instead, an approach defining separate planar fit coefficients for each 10° sector (e.g. Mammarella et al., 2007; Yuan et al., 2011) was used, resulting in a median 7% increase in flux compared with the double rotation method. This sector-wise approach does, however, introduce discontinuous adjustments at the boundaries of the somewhat arbitrarily chosen sectors. A possible solution is to define the tilt angle as a continuous function of the wind direction (Ross and Grant, 2015), but given the minor difference between the fluxes resulting from the sector planar fit and double rotation methods, the latter was chosen for this work.

Due to the Nafion™ dryer and the fixed temperature and pressure of the reaction chamber, density corrections known as WPL corrections (Webb et al., 1980) were unnecessary for determining an accurate ozone mixing ratio. However, the presence of water vapour was taken into account for the determination of ancillary parameters such as the Obukhov length used in footprint modelling. It should be noted that ~~beyond~~ in addition to its effect on mixing ratio, water vapour also quenches the chemiluminescence of the reaction of NO with O_3. This can be dealt with either by determining the instrument sensitivity over a range of water vapour conditions (at the cost of some sensitivity) and applying a correction, or by sufficiently drying the sample air. The latter approach was taken here. Despite a range of humidity (2.8×10^{-5}–1.8×10^{-2} mol/mol, Figure S1~~3~~) over the 42-day observation period, the two instruments compare well when using a fixed sensitivity for the CLD. The sensitivity value of 240 ppbv s^{-1} also compares favourably to 213 ppbv s^{-1}, which was estimated using a

Formatted: Font: (Default) +Body (Times New Roman)

supply of ~~dry~~ ozone in the absence of water vapour during lab tests prior to deployment. These results suggest that the dryer removed any major water vapour effect on the detection of ozone concentration and flux.

The sample air must travel ~~from the inlet~~ to the detector through the inlet tubing, which introduces a time lag relative to the instantaneously measured wind data. The two datasets must therefore be realigned in order to calculate the covariance. A cross-correlation function (CCF) was calculated at different time lags, with a high-pass Butterworth filter applied to the input values. The presence of a negative peak in the resulting CCF spectrum indicated a strong anticorrelation between ozone concentration and vertical wind, characteristic of deposition. Individual CCF plots were noisy, and gave scattered lag values, with a high density around 4 seconds. Daily average CCF plots indicated clear peaks in all but one case and drifted from 3.9 to 4.1 seconds over the course of the experiment (e.g. Figure 34). This is likely a consequence of slight particulate build-up in the sample line filters over the course of the measurements. Individual 20-minute flux interval lags were accepted if they fell between 3.5 and 4.5 seconds to allow for some variability in conditions (e.g. atmospheric pressure), vacuum pump strength etc. Lags that fell outside of these boundaries were then set to a value determined by a linear fit of the accepted data (Figure S25). Simply setting the lag to 4 seconds in all instances was found to decrease the flux by 5% relative to the method used here (CCF lag determination maximises the flux magnitude). The expected lag was also estimated from the inlet setup: a 13.5 L min^{-1} flow rate through 10 m of 3/8'' tubing plus a 300 mL min^{-1} sample flow through 2 m of 1/8'' tubing yields a calculated lag of 4.2 seconds ~~lag~~, similar to the CCF-determined values.

Following these steps, the ozone flux was calculated on a 20-minute basis using eddy4R (Metzger et al., 2017) with a modified workflow. Flux values were then used to determine the deposition velocity according to Eq. (1). ~~:~~

~~$v_d = \frac{F}{[O_3]}$~~ (1)

~~where v_d is deposition velocity in cm s^{-1}, F is flux in mol cm^{-2} s^{-1}, and $[O_3]$ is ozone concentration in mol cm^{-3}.~~ Molar flux was calculated using the instantaneous vertical wind, ozone mixing ratio and density of dry air. Similarly, the ozone concentration used in Eq. (1) was calculated for dry air using the mean ozone mixing ratio for the averaging period to avoid introducing a dependence on water vapour to the deposition velocity.

2.4 Data selection

A series of selection criteria were applied to the calculated 20-minute flux data. Firstly, periods with more than 10% missing data were excluded. Missing data were most commonly caused by periods of maintenance, or when heavy rain disrupted the sonic anemometer readings. Data were also selected by wind direction – only data between the true wind direction of 180° and 240° were accepted to avoid observing deposition on the headland to the north-west.

A selection criterion based on ozone variation, as used by Bariteau et al. (2010), was introduced to avoid periods of non-stationarity i.e. significantly different conditions within an averaging period (such as a sudden change in the air mass passing by the sensor, or a change in wind direction). Data were excluded if the ozone concentration drifted significantly (> 6 ppbv in 20 minutes) or if the standard deviation in ozone was above 2 ppbv. Data with a standard deviation in wind direction of >

Formatted: Space Before: 0 pt, After: 0 pt

10° were also removed to avoid non-stationarity of wind, as performed by Yang et al.~~,~~ (2016) for the same site~~. We note that the discontinuity in wind direction at for northerly winds (360° 0°) can incorrectly increase the standard deviation measured near to north. However, this issue does not arise as we consider only winds from the south-westerly sector.~~.

~~Periods of low wind speed were also excluded because of suspected land influence, as indicated by elevated deposition velocities (see Sect. 5). This is contrary to the trend of increasing deposition with wind speed proposed by Chang et al. (2004) and observed during open ocean cruises by Helmig et al. (2012). Yang et al. (2016, 2019) observed a similar enhancement in CO_2 transfer at wind speeds, and chose to filter out data when wind speeds were < 5 m s^{-1}.~~ Flux footprint analysis was used to investigate the potential for land influence within the footprint area. Land influence may increase as the footprint contracts ~~–~~during the unstable conditions coinciding most frequently with ~~at~~ low wind speeds. Using the flux footprint parameterisation of Kljun et al. (2015), footprints were calculated for each averaging period. These were defined using tide-adjusted measurement height, roughness length, friction velocity, wind speed (and direction), ~~observed~~ crosswind variability, and stability conditions, ~~and~~ then aggregated into 1 m s^{-1} wind speed bins. Using these aggregated footprints, the percentage of land area contribution in the footprint area was estimated to increase from 1–2% at high wind speeds, when atmospheric stability was predominantly neutral, to 15% at winds below 2 m s^{-1} when the atmosphere was generally unstable (Figure ~~4~~6). It should be noted that the footprint model is designed for flat homogeneous terrain – not a heterogeneous coastal site. ~~For instance, land influence may be higher than estimated at low wind speeds as a consequence of the elevation of the headland relative to sea level.~~

~~Measured r~~Roughness lengths (z_0), ~~calculated~~ derived from eddy covariance measurements using the logarithmic wind profile and Eqs. (1~~2~~–15), were also elevated at low wind speeds (Figure 5~~7~~).

$$z_0 = z/e^{\left(\frac{kU}{u_*}\Psi_m\left(\frac{z}{L}\right)\right)} \quad (12)$$

Where z_0 is roughness length in m, z is measurement height in m, κ is the von Kármán constant, U is wind speed in m s^{-1}, u_* is friction velocity in m s^{-1} (determined directly from the covariance of the fluctuations of horizontal and vertical wind components), and $\Psi_m\left(\frac{z}{L}\right)$ is the integral of the universal function (with dimensionless Obukhov stability z/L calculated from observed heat flux and u_*), defined as (Businger et al., 1971; Högström, 1988):

$$\Psi_m\left(\frac{z}{L}\right) = -6\frac{z}{L} \quad for\ \frac{z}{L} \geq 0 \quad (13)$$

$$\Psi_m\left(\frac{z}{L}\right) = ln\left[\left(\frac{1+x^2}{2}\right)\left(\frac{1+x}{2}\right)^2\right] - 2tan^{-1}x + \frac{\pi}{2} \quad for\ \frac{z}{L} < 0 \quad (14)$$

where

Formatted: Font: Italic

Formatted: Font: Italic

$$x = \left(1 - 19.3\frac{z}{L}\right)^{1/4}$$

(15)

Roughness lengths at high wind speeds are scattered approximately around 0.0002 m, which is expected for an open sea fetch (World Meteorological Organisation, 2008), but a large increase can be seen at wind speeds < 3 m s^{-1} (Figure 5). Roughness length can be slightly higher during very low wind speed, low u_* conditions (Vickers and Mahrt, 2006). However ~~T~~the scale of the increase at the PPAO is indicative of a surface with more roughness elements, such as the rocks and grass found on the headland. Greater i~~I~~naccuracies in the double rotation method at low wind speeds can mean that the removal of~~f~~ horizontal wind from the rotated vertical component is incomplete, further contributing to the elevated surface roughness values. Additionally, higher deposition velocities were observed during periods of very low winds, contrasting with the trend of increasing deposition velocity with wind speed proposed by Chang et al. (2004) and observed during open ocean cruises by Helmig et al. (2012). Yang et al. (2016, 2019) observed a similar enhancement in CO_2 transfer at low wind speeds, and chose to filter out low wind speed data. The~~is~~ above discussion indicates the need for a filter to exclude land-influenced flux data. A wind speed filter of > 3 m s^{-1} was used in this work where median fluxes and deposition velocities are reported for the whole dataset (or model work), though filters on the basis of z_0 could also be used to similar effect. ~~While it could further decrease the possibility of land influence, a more stringent filter has not been applied to avoid excessive data removal.~~

Previous eddy covariance work on CO_2 flux over land has applied filters on the basis of friction velocity ~~(u_*)~~(e.g. Barr et al., (2013)) to avoid underestimation of flux during periods of poorly developed turbulence, especially at night (Aubinet, 2008). However past measurements of oceanic ozone deposition velocity have not reported using such a filter (Gallagher et al., 2001; Helmig et al., 2012; McVeigh et al., 2010)~~, likely~~ because very low wind speeds and u_* are uncommon over the ocean. For our data, removing data with u_* < 0.1~~5~~ cm s^{-1} in addition to the criteria in Table 1 made no difference to the observed median deposition velocity. Therefore, given that a wind speed filter was already applied, no additional friction velocity filter was included.

Longer averaging periods than 20-minutes were also considered, but 60-minute averaging caused a large loss of data to the selection criteria. Missing data, as well as non-stationarity of wind and ozone ~~especially~~ contributed to an overall 23% reduction in total data accepted when using 60-minute averaging compared with 20-minute averaging. This shorter averaging time was therefore retained.~~used to avoid loss of data to stationarity requirements while still observing reasonable lag times and cospectral shape.~~

2.5 Flux uncertainty

Formatted: Space Before: 12 pt, After: 12 pt

Formatted: Font:

Flux uncertainty can be estimated in a number of ways, and in this work we make use of an empirical method (Langford et al., 2015;based on Wienhold, 1995) and a theoretical method (Fairall et al., 2000). In the method of (Langford et al., 2015),

cross-correlation functions (discussed in Sect. 2.3) are calculated at a series of improbable lag times (150–180 seconds) for each averaging period, and the root mean squared deviation of these values is taken to be representative of the random error of the flux measurement. Alternatively, the theoretical estimation of flux uncertainty of Fairall et al. (2000) can be made according to the expression:

$$\Delta F_X = \Delta\overline{w'X'} \approx \frac{\sigma_w \sigma_X}{\sqrt{T/\tau_{wca}}} \quad (16)$$

where ΔF_X is flux uncertainty, w' is instantaneous vertical wind velocity fluctuation, X' is instantaneous ozone fluctuation, σ_w is the standard deviation in vertical wind velocity, σ_X is the standard deviation in ozone concentration, T is length of the averaging period in seconds, and τ_{wca} is the integral timescale for the instantaneous covariance time series $w'X'$. A factor with a value of 1–2 is sometimes also included in the numerator of Eq. (16) to reflect uncertainty in this relationship (Blomquist et al., 2010). A factor of 1 is used in this work. The integral timescale τ_{wca} can either be determined from a flux co-spectrum peak frequency:

$$\tau_{wca} = \frac{1}{2\pi f_{max}} \quad (17)$$

or empirically according to:

$$\tau_{wca} = \frac{bz}{U} \quad (18)$$

where z is measurement height in meters, U is mean wind speed, and b is a value that varies with atmospheric stability. The value of b has been reported variably as 0.3–3 for near neutral conditions (Blomquist et al., 2010; Lenschow and Kristensen, 1985) and on the order of 10–12 for convective/unstable conditions (Blomquist et al., 2010; Fairall, 1984). The application of these methods to our data is discussed further in Sect. 3.5.

~~5~~ 3 Results

~~5~~3.1 Flux and deposition velocity values

From April 10th to May 21st, 2018, the median O_3 deposition velocity was 0.037 cm s^{-1} (interquartile range 0.017–0.063 cm s^{-1}) with a median mass flux of -0.132 mg m^{-2} h^{-1} and a median ozone concentration of 48 ppbv (Figure ~~6~~8). The resulting distribution of v_d values was compared to that obtained with the lag time set to 180s, and was ~~determined by a Kolmogorov-Smirnov test to be~~ significantly different from the results of the disjoined data (Kolmogorov-Smirnov test, $p < 0.001$; Figure S3~~10~~), rejecting the null hypothesis that the two sets of values could be taken by chance from the same distribution. This confirms that the experimental set-up used here has a sufficiently low limit of detection to discern the flux from noise over the whole duration of the measurements. The 2~~1~~σ flux uncertainty was determined for each 20-minute period (see Sect. 3.5~~5~~.4), with a median uncertainty of 0.113 mg m^{-2} h^{-1}, corresponding to a deposition velocity uncertainty of 0.031 cm s^{-1}. A

typical single flux observation is therefore above the 2σ limit of detection, albeit with considerable uncertainty, although ~~T~~this uncertainty reduces with the square root of the sample size where ~~aggregated~~ averaged results are presented.

Previous eddy covariance ozone deposition velocity measurements have yielded values of 0.009–0.034 cm s^{-1} over five open ocean cruises (Helmig et al., 2012) with higher values typically corresponding to warmer oceans. Additionally, tower-based measurements have reported deposition velocities at coastal locations to be 0.025 cm s^{-1} (McVeigh et al., 2010), 0.030 cm s^{-1} (Whitehead et al., 2009) and 0.13 cm s^{-1} (Gallagher et al., 2001). These measurements were carried out at Mace Head (west Ireland), Weybourne (east UK) and Roscoff (north-west France) respectively. Our median v_d of 0.037 cm s^{-1} is towards the upper end of previous work, though much lower than Gallagher et al. (2001).

~~5~~3.2 Wind ~~s~~Speed ~~d~~Dependence

Reports on t~~T~~he dependence of v_d on wind speed and friction velocity (u_*) vary considerably; the cruise observations discussed by ~~(~~Helmig et al.~~,~~ (2012) vary from strong to zero dependence, while both ~~(~~McVeigh et al.~~,~~ (2010) and ~~(~~Gallagher et al.~~,~~ (2001) observe tentative relationships. We examine this relationship for our data~~is examined~~ in Figure ~~8~~11A ~~and B~~. Individual values that passed the filtering criteria exhibit a large degree of scatter, and are therefore presented alongside median values within wind speed bins of 1 m s^{-1} ~~and friction velocity bins of 0.05 m s^{-1}~~. Note that v_d values removed by the wind speed filter (Sect. 2.4) are shown in the shaded region of Figure ~~8~~11A ~~to~~ and demonstrate the ~~increase~~ elevated ~~of~~ v_d at low wind speeds~~, but are excluded from Figure 11B~~. Outside of the excluded low wind speed region, v_d values are relatively constant up to 10 m s^{-1}. Above 10 m s^{-1}, v_d begins to increase, though data are sparse above 14 m s^{-1}.

The wind speed dependency of v_d has been discussed in a number of other studies. Chang et al. (2004) report a five-fold increase in v_d (0.0158–0.0775 cm s^{-1}) from 0 to 20 m s^{-1}, with v_d near constant below 4 m s^{-1}, and approximately doubling from 4–10 m s^{-1}. Tower-based eddy covariance measurements by Gallagher et al. (2001) exhibit increasing ozone deposition velocity as wind speed increases, with v_d tripling over the range u_* = 0.05–0.5 m s^{-1}. Using the same type of instrument, McVeigh et al. (2010) report a similar trend, fitting an exponential curve to their data. Lastly, deposition velocity during two of the five cruises reported by Helmig et al. (2012) increases with increasing wind speeds. The dependence observed in our data is discussed further in Sect. 4.2.~~These data fit reasonably well to the parameterisation of Fairall et al. (2007):~~

~~$$v_d \cong \alpha\sqrt{AD_c} + \frac{\alpha}{6}\kappa u_{*w} \quad (6)$$~~

~~where α is the dimensionless solubility of ozone in water, A is the effective rate constant for the reaction of ozone with molecules in the surface water in s^{-1}, D_c is the molecular diffusion coefficient of ozone in water in m^2 s^{-1}, κ is the von Kármán constant (0.4), and u_{*w} is the water-side friction velocity in m s^{-1}. The fit shown in blue in Figure 11B was determined using the relevant parameters during the experiment at the PPAO, with u_{*w} derived from u_* using:~~

~~$$u_{*w} = \sqrt{\frac{\rho_{air}}{\rho_{water}}}u_* \quad (7)$$~~

~~**Formatted:** Space Before: 0 pt, After: 0 pt~~

~~**Formatted:** Space Before: 0 pt, After: 0 pt~~

where ρ_{air} and ρ_{water} are the densities of air and water respectively. α, A, and D_c were determined empirically according to Eq. (8) (Morris, 1988), Eq. (9) (Magi et al., 1997), and Eq. (10) (Johnson and Davis, 1996):

$$\alpha = 10^{-0.25-0.013(T_s-273.16)} \quad (8)$$

$$A = [I^-]e^{\left(\frac{-8772.2}{T_s}+51.5\right)} \quad (9)$$

$$D_c = 1.1 \times 10^6 e^{\left(\frac{-1896}{T_s}\right)} \quad (10)$$

where T_s is the sea surface temperature (in K) and $[I^-]$ is the aqueous iodide concentration in mol dm^{-3}. We note that Eq. (9) only accounts for the reactivity of ozone with iodide in the sea surface. Other species present in the SML have also been shown to react with ozone (Martino et al., 2009; Shaw and Carpenter, 2013), but given the uncertainty surrounding their rate constants and any temperature dependence, they have been omitted here. Fixed T_s (284 K) and $[I^-]$ (85 nmol dm^{-3}) values from the relevant period and representative of the footprint of PPAO (Sherwen et al., 2019) were used to determine α, A, and D_c, and thus v_d (cm s^{-1}) using Eq. (6) (shown in blue on Figure 11B). This can be simplified to:

$$v_{d\,predicted} = 0.01324 + 0.09378u_*$$

In comparison, the linear fit of our experimental 20-minute v_d values against u_* is:

$$v_{d\,measured} = 0.02017 + 0.07537u_*$$

Our results therefore show comparable, but slightly lower dependence on friction velocity (and therefore also wind speed) than predicted by the parameterisation of Fairall et al. (2007). Given the assumptions of the simplified model (Eq. (6)) and the uncertainties in various parameters, not least the rate constant for the reaction of O_3 with I^- (e.g. Moreno & Baeza-Romero, 2019), this agreement is remarkable. The two-layer model of Luhar et al. (2018) for the same data is shown in black in Figure 11B. Considering only iodide reactivity, this model appears to under-predict deposition compared with the one-layer model of Fairall et al. (2007), and lacks any major dependence on wind speed except during very calm conditions (see Sect. 6 for further discussion).

53.3 Land and Tidal iInfluence

Aggregate flux fFootprint analysis of the PPAO site (as discussed in Sect. 2.4) suggests that the spatial contribution of land surfaces to our observed deposition velocity is approximately 3.9% (Figure 9). However, deposition velocity totto land is typically greater than to the ocean, amplifying the potential influence of land deposition on our data. If our observations were adjusted for 3.9% spatial contribution of grassland ($v_d \approx 0.25$ cm s^{-1}, median land deposition value from datasets analysed by Hardacre et al., (2015)), then our calculated median coastal water v_d would be 0.028 cm s^{-1} (23% lower than we measured). In reality the terrain is a mixture of grassland and rocky shoreline, varying in extent with the tide, so the land v_d discussed above may be an overestimate. It should also be noted that the grassland deposition velocity value used here is itself prone to considerable uncertainty due to the variability of the datasets used in the model. Although there are insufficient data over the land to the north-west to reliably determine a v_d value for to the land around the PPAO, an estimate can be made by

Formatted: Space Before: 0 pt, After: 0 pt

Formatted: Space Before: 0 pt, After: 0 pt

Formatted: Space Before: 0 pt, After: 0 pt

Field Code Changed

obtaining a least square solution using the land cover determined in Figure ~~4~~6 and the observed v_d values in Figure ~~8~~11~~A~~. Data from wind speeds > 14 m s^{-1} were not used (only 4 data points). Using all data from 2–13 m s^{-1} yielded values of 0.167 ± 0.080 cm s^{-1} and 0.034 ± 0.016 cm s^{-1} for land and sea respectively, suggesting a lesser effect from land than using the fixed value from Hardacre et al. (2015). Given that the land contribution in Figure ~~4~~6 doesn't stabilise until 9 m s^{-1}, it is possible that constant v_d between 4 and 10 m s^{-1} wind speeds (Figure ~~8~~11~~A~~) may be a consequence of land influence and wind speed enhancement counteracting one another. Estimated water-only v_d values, calculated by subtracting the product of the land fraction and the land v_d value from the measured v_d, are shown in Figure 1~~0~~3.

It is worth reiterating that ~~this~~ the Kljun footprint model is designed for use in homogenous environments, which is not ~~true~~ the case for ~~of~~ our site. ~~-~~Furthermore, the double rotation applied to the wind data will result in varying pitch angles relative to the water surface, introducing a dependence of the footprint extent on this pitch angle. These limitations may be important for work relying on direct interpretations of the flux footprint, such as comparisons to emissions inventories (Squires et al., 2020; Vaughan et al., 2017). In contrast to an inventory comparison, we only use the flux footprint model to develop a strategy for robust data selection, and generate an aggregate footprint from several individual footprints. ~~use aggregates of these individual footprints only to develop a strategy for robust data selection.~~This approach follows the works of ~~(~~Amiro~~,~~ (1998)~~);~~ Göckede et al.~~,~~ (2006, 2008); Kirby et al.~~,~~ (2008)~~);~~ Metzger~~,~~ (2018)~~);~~ and Xu et al.~~,~~ (2018) who have demonstrated the utility of aggregation for deriving robust footprint-based metrics in heterogeneous environments.

3.4 Tidal influence

The PPAO site flux footprint also experiences periodic variations associated with the tide, which alters the effective measurement height and changes the land type in the footprint when the shoreline is exposed. Whitehead et al. (2009) provide an extreme example of this, reporting v_d increasing from 0.030 cm s^{-1} at high tide to 0.21 cm s^{-1} at low tide during the day~~. at a site with a tidal range of 9 m~~ This large variation in their work was a consequence of a 9 m tidal range exposing the sea floor up to 3 km from the shore. At Penlee, ~~T~~the tide also causes periodic movement of the river plume around the ~~Penlee~~ headland, altering the salinity and composition of the surface water (Yang et al., 2016). ~~-~~This altered composition could affect the reactivity of ozone at the sea surface. Such effects will be examined in future ~~Measurement~~ work. Tower height above the water was ~~adjusted~~ determined~~for tide height~~ for all flux calculations using tidal data from the British Oceanographic Data Centre (BODC), measured approximately 6 km upstream. Periodograms were also used to look for periodic ~~deposition~~ variation in deposition velocity from exposed shoreline or riverine water, but none could be identified above the variability in the data. We note that previous measurements of air-sea exchange of momentum (Yang et al., 2016a), CO_2 (Yang et al., 2019a) and sea spray (Yang et al., 2019b) at the PPAO were also unable to identify tidal cycles in the data. Gallagher et al. (2001) report a tentative (though statistically insignificant) diurnal cycle for coastal water during observations made at Weybourne in East Anglia, UK. However, no ~~such~~ diurnal variability~~trend~~

Formatted: Space Before: 12 pt, After: 12 pt

was observed in the PPAO O_3 flux data (as might be expected due to deposition to land), again implying minimal land influence in our filtered observations.

~~5.4~~3.5 Measurement ~~u~~uncertainty

To understand the variability in our v_d observations, a flux limit of detection was obtained empirically according to the method of Langford et al. (2015) (Sect. 2.5). ~~For each averaging period, cross-correlation functions (discussed in Sect. 3) were calculated at a series of improbable lag times (150–180 seconds), and the root mean squared deviation of these values was taken to be representative of the random error of the flux measurement.~~ Limits of detection were calculated for each averaging period due to its dependence on wind speed and atmospheric stability, giving a median 2σ flux limit of detection of 0.113 mg m^{-2} h^{-1}. At the average ozone concentration of 48 ppbv, this equates to a deposition velocity of 0.03~~1~~3 cm s^{-1}, with 305 of the 491 averaging periods exceeding their individually determined 2σ limit of detection.

~~Alternatively, a theoretical estimation of flux uncertainty can be made according to the expression given by Fairall et al. (2000):~~

$$\Delta F_{\chi} = \Delta\overline{w'\chi'} \approx \frac{\sigma_w \sigma_\chi}{\sqrt{T/\tau_{wc\alpha}}} \quad (11)$$

~~where ΔF_{χ} is flux uncertainty, w' is instantaneous vertical wind velocity fluctuation, X' is instantaneous ozone fluctuation, σ_w is the standard deviation in vertical wind velocity, σ_χ is the standard deviation in ozone concentration, T is length of the averaging period in seconds, and $\tau_{wc\alpha}$ is the integral timescale for vertical fluctuations. A factor with a value of 1–2 is sometimes also included to reflect uncertainty in this relationship (Blomquist et al., 2010). The integral timescale $\tau_{wc\alpha}$ can either be determined from a flux cospectrum peak frequency:~~

$$\tau_{wc\alpha} = \frac{1}{2\pi f_{max}} \quad (12)$$

~~or empirically according to:~~

$$\tau_{wc\alpha} = \frac{\alpha z}{U} \quad (13)$$

~~where z is measurement height in meters, U is mean wind speed, and α is a value that varies with atmospheric stability. The value of α has been reported variably as 0.3–3 for near neutral conditions (Blomquist et al., 2010; Lenschow and Kristensen, 1985) and on the order of 10–12 for convective/unstable conditions (Blomquist et al., 2010; Fairall, 1984). Using~~ To determine a theoretical uncertainty using Eq. (16), the peak frequency of the co-spectrum shown in Figure 1~~1~~4 (0.07 Hz), was used to determine τ_{wca} ~~was determined to be~~ as approximately 2.2 s during near-neutral conditions and wind speeds of 12.1 m s^{-1}. Using Eq. (17) and Eq. (18), ~~T~~this corresponds to a value for $b\alpha$ of 1.5, similar to the literature values for near neutral conditions (Blomquist et al., 2010; Lenschow and Kristensen, 1985). Since individual 20-minute co-spectra were too noisy, this $b\alpha$ value was used with Eq. (18~~13~~) to determine τ_{wca} for each 20-minute period. It should be noted that the value

of $b\sigma$ is stability dependent. However, since stability was near neutral for most periods (z/L = -0.39 to 0.15, 20th–80th percentile), the effects of varying stability on $b\sigma$ are expected to be small.

Using these integral timescales, a theoretical flux uncertainty can be calculated for each averaging period using Eq. (1611). The theoretical values obtained were much higher than those found empirically – the median theoretical 2σ limit of detection was 0.241 mg m^{-2} h^{-1} compared with the empirical value of 0.113 mg m^{-2} h^{-1}. We note however that this is an approximation, derived from the work of Lenschow & Kristensen (1985) who defined multiplied twice the right-hand side of Eq. (1611) by 2 to derive be an upper limit on flux uncertainty.

Equation (1116) demonstrates how the variability of ozone and vertical wind within averaging intervals are directly related to uncertainty in the measured flux. White noise in the wind measurement is expected to be very small, such that whereas random instrument noise in the ozone instrument likely represents a significant contribution to the total variance of ozone observed at 10 Hz. Given the relatively low sensitivity of the instrument used in this work (240 counts ppbv $^{-1}$ s^{-1} compared to 2800 counts ppbv^{-1} s^{-1} reported by Helmig et al. (2012)), autocovariances were calculated for each averaging period using the 10 Hz ozone data to examine the extent to which variance in ozone concentration is caused by instrument white noise. White noise only correlates with itself at zero lag time, so it can be estimated from the difference between the first and second points in an autocovariance plot (Blomquist et al., 2010). Instrument white noise derived using this approach was found to contribute 45–98% to the total ozone variance (10th–90th percentile), with a median σ_{noise} of 1.4 ppbv. A more sensitive ozone instrument could therefore significantly improve the flux uncertainty at a 20-minute averaging period.

Besides the random uncertainty discussed above, systematic errors are also worthy of some consideration. Specifically, whether the highest and lowest frequencies of turbulence have been adequately observed. High frequency information can be lost if measurements are made too infrequently, or if the sample is attenuated significantly in the sample linetubing. Measurements at 10 Hz, as performed here, are widely considered sufficient to observe this high frequency structure. Sensor separation was minimised by locating the sample inlet directly beneath the sonic anemometer (~20 cm below). Laminar flow was also avoided through the length of the sample line (Reynolds number = 3000). As a result, the co-spectrum in Figure 114 shows no major loss of high frequency information compared to theory. Since fluxes were calculated over 20-minute averaging periods using linear detrending, there is also a chance that low frequency information may not be fully observed. Firstly, using a simple block average in place of linear detrending had little effect on the median flux observed (+1.7%), implying that linear detrending is not causing much low frequency information loss. Using an averaging period of 1 hour instead of 20 minutes gave slightly larger magnitude flux (+4.1%) as well. However, the longer period lead to much greater data loss (22%) to the selection criteria in Sect. 2.4, hence the 20-minute average was used for this work. This suggests that any low frequency loss is approximately 5% of the total flux – a small amount relative to the calculated 2σ random uncertainty (85%).

6 4 Discussion

4.1 Model comparison

For the average meteorological conditions observed during this work, the one-layer model of Fairall et al. (2007) predicts a deposition velocity of 0.037 cm s^{-1}, assuming reaction of ozone with iodide only. Here, one-layer refers to considering the surface water column to have uniform reactivity to ozone with depth, rather thanThis is not the same as a thin sublayer at the surface where reactivity is enhanced considering the chemical reaction only in the reaction-diffusion sublayer, and both chemical reaction and turbulent transfer in the layer beneath (thea two-layer model). By contrast, the revised two2-layer model of Luhar et al. (2018) predicts a deposition velocity of 0.0186 cm $^{-1}$ for the same conditions using a fixed reaction-diffusion sublayer (δ_m) of 4.23 µm, parameterized using Eq. (11).. An iodide concentration of ~600 nmol dm^{-3} would be necessary to yield the observed deposition velocity – much higher than a typical oceanic value of 77 ~80 nmol dm^{-3} (Chance et al., 2014). However, DOM (Shaw and Carpenter, 2013), chlorophyll (Clifford et al., 2008) and surfactants (McKay et al., 1992) have also been shown to enhance increase ozone deposition velocity. Therefore the effective pseudo-first order rate constant for the reaction of ozone with water, aA, is likely to be significantly higher than accounted for by iodide alone in Eq. (9). Chang et al. (2004) defined this total reactivity as:

$$aA = \sum_i k_i C_i \quad (14\,19)$$

Where aA is the effective pseudo-first order rate constant for the reaction of ozone with water, and k_i and C_i are the second order rate constant and concentration of species i, respectively. We can therefore include an estimate of the effects of DOM reactivity using a typical oceanic DOM concentration of 52 µmol dm^{-3} (Massicotte et al., 2017) and a rate constant of 3.7×10^{-6} dm^3 mol^{-1} s^{-1} (average of the values reported by Sarwar et al. (2016) and Coleman et al. (2010)). Doing so increases A a from 544 s^{-1} to 737 s^{-1} and leads to increased average deposition values velocities for our field campaign of 0.048 cm s^{-1} and 0.028 cm s^{-1} for the models of Fairall and Luhar, respectively.

The magnitude of the effect of DOM on O_3 deposition velocity remains highly uncertain due to the uncertainties in how O_3 interacts with DOM and surfactants, variability in the sea-surface microlayer (SML) composition, and the effect of temperature. The coastal waters near the PPAO experience large phytoplankton growth during the 'spring bloom' (Cushing, 1959; Smayda, 1998), and the organic content and composition of the SML could be very different compared to the open ocean. The seasonal and spatial variations in these O_3-reactive substances could, in turn drive differences in ozone deposition velocity. For example, Bariteau et al. (2010) reported v_d increasing from 0.034 cm s^{-1} to 0.065 cm s^{-1} as the waters changed from open ocean into coastal during the TexAQS-2006 cruise. It is unclear how much of the observed gradient is a result of SML composition or of terrestrial influence. Similarly, the model of Ganzeveld et al. (2009) encountered underestimatedion of coastal ozone deposition velocities in their modelling work when DOM reactivity was omitted, suggesting that this may be a particularly important factor in coastal environments. While the model of Fairall et al.

Formatted: Font: Italic

(2007) appears to match our observed v_d well, it is possible that this is a consequence of some missing reactivity. Inclusion of DOM causes the one-layer model to overestimate v_d, as reported by Luhar et al. (2018).

4.2 Wind speed dependence

In their discussion on wind speed dependence, ~~(~~Helmig et al.~~,~~ (2012) found their data fit reasonably well with the parameterisation of Fairall et al. (2007):

$$v_d \cong \alpha\sqrt{aD_c} + \frac{\alpha}{6}\kappa u_{*w} \quad (20)$$

where α is the dimensionless solubility of ozone in water, a is the effective rate constant for the reaction of ozone with molecules in the surface water in s^{-1}, D_c is the molecular diffusion coefficient of ozone in water in $m^2\ s^{-1}$, κ is the von Kármán constant (0.4), and u_{*w} is the water-side friction velocity in $m\ s^{-1}$. The fit shown in blue in Figure 12 was determined using parameter values relevant to the experiment at the PPAO, with u_{*w} derived from u_* assuming atmospheric surface stress to be equal to the waterside surface stress (Luhar et al., 2017):

$$u_{*w} = \sqrt{\frac{\rho_{air}}{\rho_{water}}}u_* \quad (21)$$

where ρ_{air} and ρ_{water} are the densities of air and water respectively. α, a, and D_c were determined empirically according to Eq. (22) (Morris, 1988), Eq. (23) (Magi et al., 1997), and Eq. (24) (Johnson and Davis, 1996):

$$\alpha = 10^{-0.25-0.013(T_s-273.16)} \quad (22)$$

$$a = [I^-]e^{\left(\frac{-8772.2}{T_s}+51.5\right)} \quad (23)$$

$$D_c = 1.1 \times 10^6 e^{\left(\frac{-1896}{T_s}\right)} \quad (24)$$

where T_s is the sea surface temperature (in K) and $[I^-]$ is the aqueous iodide concentration in mol dm^{-3}. We note that Eq. (23) only accounts for the reactivity of ozone with iodide in the sea surface. Other species present in the SML have also been shown to react with ozone (Martino et al., 2009; Shaw and Carpenter, 2013), but given the uncertainty surrounding their reactivity and any temperature dependence, they have been omitted here. Fixed T_s (284 K) and $[I^-]$ (85 nmol dm^{-3}) values from April-May 2018 and representative of the footprint of PPAO (Sherwen et al., 2019) were used to determine α, a, and D_c, and thus v_d (cm s^{-1}) using Eq. (20) (blue dashed line in Figure 12). This can be simplified to:

$$v_{d\ predicted} = 0.01324 + 0.09378u_*$$

In comparison, the linear fit (red dashed line in Figure 12) of our experimental 20-minute v_d values against u_* (with standard errors) is:

Formatted: Space Before: 12 pt, After: 12 pt

$v_{d\ measured} = (0.02017 \pm 0.00570) + (0.07537 \pm 0.01953)u_*$

Our results therefore show comparable, but slightly lower dependence on friction velocity (and therefore also wind speed) than predicted by the parameterisation of Fairall et al. (2007). Comparison of our data to this parameterisation yielded a root mean square error (RMSE) of 0.0522 cm $^{-1}$ and a mean bias of 0.0020 cm s^{-1} (a positive bias here denoting observations greater than the model). Given the assumptions of the simplified model (Eq. (20)) and the uncertainties in various parameters, not least the rate constant for the reaction of O_3 with I^- (e.g. Moreno & Baeza-Romero, 2019), this agreement is perhaps surprising. The two-layer model of Luhar et al. (2018) for the same data is shown in black in Figure 12. Considering only iodide reactivity (i.e. omitting any enhancement in reaction rate due to the presence of organic material in both models), this model appears to under-predict deposition velocity compared with the one-layer model of Fairall et al. (2007), and lacks any major dependence on wind speed except during very calm conditions. Comparison of our data to the two-layer model gave higher RMSE and mean bias (0.0584 cm s^{-1} and 0.0247 cm s^{-1} respectively).

~~If the two-layer model provides more accurate deposition velocities with adequate reactivity information, then it shows little dependence upon wind speed in all but the calmest conditions. This would stand in contrast to the one-layer model, and a number of experimental observations including those presented here.~~The two-layer model is set up to account for ozone reactions with chemical species other than iodide. Inclusion of these additional reactions would increase the predicted deposition velocity to be more similar to our observations. However, the two-layer model also predicts that v_d does not strongly depend upon variations in wind speed, which is in contrast with our observations.

~~7~~ 5 Summary and conclusions

An ozone chemiluminescence detector adapted from an Eco Physics® CLD 886 NO_x detector was used to measure the ozone deposition velocity to the sea surface at a coastal site near Plymouth, on the southwest coast of the UK. The median observed deposition velocity was 0.037 cm s^{-1}, comparable with previous values from tower-based measurements of 0.025 cm s^{-1} (McVeigh et al., 2010) and 0.030 cm s^{-1} (Whitehead et al., 2009).~~past work,~~ Furthermore, our data are ~~but~~ at the upper end of the values obtained by Helmig et al. (2012) during ship-based, open-ocean measurements (0.009–0.034 cm^{-1}). Cross-covariance was used to empirically determine a 2σ limit of detection for the O_3 flux for each averaging period. This limit of detection had a median value of 0.113 mg m^{-2} h^{-1}, and was exceeded in 305 out of 491 flux intervals. Auto-covariance of high-frequency ozone data indicated that instrument noise was a significant component in the observed ozone variability (45-98%), and lowering the noise level would reduce the flux uncertainty.

In moderate to high winds, the observed deposition velocity showed a linear dependence on friction velocity in the mean. This is comparable to that predicted by the one-layer model of Fairall et al. (2007) considering only ozone-iodide reaction.

However, including estimated (but unverified) contributions from ozone-DOM reactions causes the one-layer model to overpredict the observations.

For the conditions encountered during the campaign, the two-layer model of Luhar et al. (2018) yields a predicted v_d of 0.018 cm s^{-1} with iodide reaction only, and 0.026 cm s^{-1} with reactions of both iodide and estimated contributions from DOM. While the latter value is close to our median observation, the two-layer model does not reproduce the observed wind speed dependence in v_d.

~~Using observed meteorology with the model of Luhar et al. (2018) yields a predicted v_d of 0.018 cm s^{-1} in the absence of DOM reactivity, or 0.026 cm s^{-1} with estimated DOM concentration of 52 μmol dm^{-3} and a O_3 + DOM rate constant of 3.7 × 10^{-6} dm^3 mol^{-1} s^{-1}. We suspect that the difference from our measured v_d is due to the uncertainty surrounding the reaction between O_3 and DOM, and the timing of our measurements, which coincide with the spring bloom and potential enhancements in surface microlayer reactive organics.~~

Elevated deposition velocities w~~ereas~~ observed at low wind speeds, contrary to predictions (Chang et al., 2004) and to previous observations (Helmig et al., 2012). We attribute this observation to a contribution to v_d from land within the footprint during periods of low wind. Periods with wind speeds > 3 m s^{-1} (corresponding to approximately < 10% land cover in the footprint) were used to evaluate v_d. However, the possibility of land influence could not be completely removed, with our oceanic v_d estimates potentially overestimated by 8%, even after wind speed filtering. ~~Deposition velocity showed a linear dependence on friction velocity comparable to that predicted by the parameterisation of Fairall et al. (2007), though with considerable scatter.~~ The potential for tidal effects on v_d (exposing shoreline and input of river water with different chemical composition) were also examined, though no clear periodicity could be observed, either at the tidal frequency or on a diurnal timescale.

~~Cross-covariance was used to empirically determine a 2σ limit of detection for each averaging period. This limit of detection was exceeded in 305 out of 491 periods. Auto-covariance of high-frequency ozone data indicated that instrument noise was a significant component in the observed ozone variability, and lowering the noise level would reduce the flux uncertainty.~~

Future work will link the properties of the sea-surface microlayer in the footprint area to observed O_3 fluxes. A ~~larger~~ longer ~~dataset~~ time series with more observations of microlayer chemical composition may help to elucidate the influence of biogeochemical parameters, seasonal variation and wind speed dependence, which have not been definitively characterised to date.

Code and data availability: the eddy4R software packages used in these analyses are maintained at https://github.com/NEONScience/NEON-FIU-algorithm. 20-minute data have been submitted to the Centre for Environmental Data Analysis (CEDA), ~~awaiting DOI~~doi:10.5285/8351ed155b134155848d03a7cdce9f02. The corresponding author can be contacted directly for the full high-frequency data.

Author contribution: Experimental work was carried out by DCL, TGB and MY. DCL also conducted the formal analysis and visualisation of the results, with relevant supervision from TGB and MY. SM developed the eddy4R codebase, with ARV providing modification for its use here. RJP provided software for instrumentation and validation of model

applications to the data. JDL and LJC supervised the interpretation of the results. The work was proposed by LJC, who also acquired the necessary funding. DCL pPrepared the manuscript with all authors contributing to the editing process.

Competing interests: The authors declare that they have no conflict of interest.

~~8~~ 6 Acknowledgements

LJC and DCL thank funding from the Natural Environment Research Council (NERC), UK, through the grant "Iodide in the ocean: distribution and impact on iodine flux and ozone loss" (NE/N009983/1). DCL also thanks NERC for the funding of his PhD project (NERC SPHERES DTP NE/L002574/1). LJC acknowledges funding from the European Research Council (ERC) under the European Union's horizon 2020 programme (Grant agreement No. 833290, O3-SML). The National Ecological Observatory Network is a project sponsored by the National Science Foundation and managed under co-operative agreement by Battelle. This material is based upon work supported by the National Science Foundation (Grant DBI-0752017). Any opinions, findings, and conclusions or recommendations expressed in this material are those of the author and do not necessarily reflect the views of the National Science Foundation. Trinity House (https://www.trinityhouse.co.uk/, accessed 10/1/20) owns the Penlee Point Atmospheric Observatory (PPAO) site, who allow Plymouth Marine Laboratory (PML) use the building to house instrumentation. Access to the site is arranged thanks to Mount Edgcumbe Estate (https://www.mountedgcumbe.gov.uk/, accessed 10/1/20). PPAO research (including the contributions of T.G.B. and M.Y. to this manuscript) is supported by NERC via the national capability ACSIS project (grant no. NE/N018044/1). We thank Frances Hopkins (PML), Daniel Philips (University of East Anglia) and Oban Jones (PML) for assistance at the field site. This work is contribution number 8 from the PPAO. ~~The National Ecological Observatory Network is a project sponsored by the National Science Foundation and managed under co-operative agreement by Battelle. This material is based upon work supported by the National Science Foundation (Grant DBI-0752017). Any opinions, findings, and conclusions or recommendations expressed in this material are those of the author and do not necessarily reflect the views of the National Science Foundation.~~

References

Aldaz, L.: Flux Measurements of Atmospheric Ozone Over Land Water, J. Geophys. Res., 74(28), 6943–6946, 1969.

Amiro, B. D.: Footprint climatologies for evapotranspiration in a boreal catchment, Agric. For. Meteorol., 90(3), 195–201, doi:10.1016/S0168-1923(97)00096-8, 1998.

Aubinet, M.: Eddy Covariance CO2 Flux Measurements in Nocturnal Conditions: an Analysis of the Problem, Ecol. Appl., 18(6), 1368–1378, 2008.

Bariteau, L., Helmig, D., Fairall, C. W., Hare, J. E., Hueber, J. and Lang, E. K.: Determination of oceanic ozone deposition by ship-borne eddy covariance flux measurements, Atmos. Meas. Tech., 3(2), 441–455, doi:10.5194/amt-3-441-2010, 2010.

Barr, A. G., Richardson, A. D., Hollinger, D. Y., Papale, D., Arain, M. A., Black, T. A., Bohrer, G., Dragoni, D., Fischer, M. L., Gu, L., Law, B. E., Margolis, H. A., Mccaughey, J. H., Munger, J. W., Oechel, W. and Schaeffer, K.: Use of change-point detection for friction-velocity threshold evaluation in eddy-covariance studies, Agric. For. Meteorol., 171–172, 31–45, doi:10.1016/j.agrformet.2012.11.023, 2013.

Blomquist, B. W., Huebert, B. J., Fairall, C. W. and Faloona, I. C.: Determining the sea-air flux of dimethylsulfide by eddy correlation using mass spectrometry, Atmos. Meas. Tech., 3(1), 1–20, doi:10.5194/amt-3-1-2010, 2010.

Brock, F. V.: A Nonlinear Filter to Remove Impulse Noise from Meteorological Data, J. Atmos. Ocean. Technol., 3(1), 51–58, doi:10.1175/1520-0426(1986)003<0051:anftri>2.0.co;2, 1986.

Businger, J. A., Wyngaard, J. C., Izumi, Y. and Bradley, E. F.: Flux- profile relationships in the atmospheric surface layer, J. Atmos. Sci., 28(2), 181–189, 1971.

Chance, R., Baker, A. R., Carpenter, L. and Jickells, T. D.: The distribution of iodide at the sea surface., Environ. Sci. Process. Impacts, 16, 1841–1859, doi:10.1039/c4em00139g, 2014.

Chance, R. J., Tinel, L., Sherwen, T., Baker, A. R., Bell, T., Brindle, J., Campos, M. L. A. M., Croot, P., Ducklow, H., Peng, H., Hopkins, F., Hoogakker, B., Hughes, C., Jickells, T. D., Loades, D., Macaya, D. A. R., Mahajan, A. S., Malin, G., Phillips, D., Roberts, I., Roy, R., Sarkar, A., Sinha, A. K., Song, X., Winkelbauer, H., Wuttig, K., Yang, M., Peng, Z. and Carpenter, L. J.: Global sea-surface iodide observations, 1967-2018, Sci. data, 6(1), 286, doi:10.1038/s41597-019-0288-y, 2019.

Chang, W., Heikes, B. G. and Lee, M.: Ozone deposition to the sea surface: Chemical enhancement and wind speed dependence, Atmos. Environ., 38(7), 1053–1059, doi:10.1016/j.atmosenv.2003.10.050, 2004.

Clifford, D., Donaldson, D. J., Brigante, M., D'Anna, B. and George, C.: Reactive uptake of ozone by chlorophyll at aqueous surfaces, Environ. Sci. Technol., 42(4), 1138–1143, doi:10.1021/es0718220, 2008.

Coleman, L., Varghese, S., Tripathi, O. P., Jennings, S. G. and O'Dowd, C. D.: Regional-Scale Ozone Deposition to North-East Atlantic Waters, Adv. Meteorol., 2010, 1–16, doi:10.1155/2010/243701, 2010.

Cushing, D. H.: The seasonal variation in oceanic production as a problem in population dynamics, ICES J. Mar. Sci., 24(3), 455–464, doi:10.1093/icesjms/24.3.455, 1959.

Fairall, C. W.: Interpretation of eddy-correlation measurements of particulate deposition and aerosol flux, Atmos. Environ., 18(7), 1329–1337, 1984.

Fairall, C. W., Hare, J. E., Edson, J. B. and McGillis, W.: Parameterization and Micrometeorological Measurement of Air-Sea Gas Transfer., 2000.

Fairall, C. W., Helmig, D., Ganzeveld, L., Hare, J. and Science, E.: Water-side turbulence enhancement of ozone deposition to the ocean, Atmos. Chem. Phys., 443-451 ST-Water-side turbulence enhancement of, 2007.

Foken, T.: Micrometeorology, 1st ed., Springer-Verlag Berlin Heidelberg., 2008.

Galbally, I. E. and Roy, C. R.: Destruction of ozone at the earth's surface, Q. J. R. Meteorol. Soc., 106(449), 599–620, doi:10.1002/qj.49710644915, 1980.

Gallagher, M. W., Beswick, K. M. and Coe, H.: Ozone deposition to coastal waters, Q. J. R. Meteorol. Soc., 127(October 1999), 539–558, doi:10.1002/qj.49712757215, 2001.

Ganzeveld, L., Helmig, D., Fairall, C. W., Hare, J. and Pozzer, A.: Atmosphere-ocean ozone exchange: A global modeling study of biogeochemical, atmospheric, and waterside turbulence dependencies, Global Biogeochem. Cycles, 23(4), 1–16, doi:10.1029/2008GB003301, 2009.

Garland, J. A., Elzerman, A. W., Penkett, A. A.: The mechanism for dry deposition of ozone to seawater surface, J. Geophys. Res., 85, 7488–7492, 1980.

Göckede, M., Markkanen, T., Hasager, C. B. and Foken, T.: Update of a footprint-based approach for the characterisation of complex measurement sites, Boundary-Layer Meteorol., 118(3), 635–655, doi:10.1007/s10546-005-6435-3, 2006.

Göckede, M., Foken, T., Aubinet, M., Aurela, M., Banza, J., Bernhofer, C., Bonnefond, J. M., Brunet, Y., Carrara, A., Clement, R., Dellwik, E., Elbers, J., Eugster, W., Fuhrer, J., Granier, A., Grünwald, T., Heinesch, B., Janssens, I. A., Knohl, A., Koeble, R., Laurila, T., Longdoz, B., Manca, G., Marek, M., Markkanen, T., Mateus, J., Matteucci, G., Mauder, M., Migliavacca, M., Minerbi, S., Moncrieff, J., Montagnani, L., Moors, E., Ourcival, J. M., Papale, D., Pereira, J., Pilegaard, K., Pita, G., Rambal, S., Rebmann, C., Rodrigues, A., Rotenberg, E., Sanz, M. J., Sedlak, P., Seufert, G., Siebicke, L., Soussana, J. F., Valentini, R., Vesala, T., Verbeeck, H. and Yakir, D.: Quality control of CarboEurope flux data - Part 1: Coupling footprint analyses with flux data quality assessment to evaluate sites in forest ecosystems, Biogeosciences, 5(2), 433–450, doi:10.5194/bg-5-433-2008, 2008.

Hardacre, C., Wild, O. and Emberson, L.: An evaluation of ozone dry deposition in global scale chemistry climate models, Atmos. Chem. Phys., 15(11), 6419–6436, doi:10.5194/acp-15-6419-2015, 2015.

Heck, W. W., Taylor, O. C., Adams, R., Bingham, G., Miller, J., Preston, E. and Weinstein, L.: Assessment of Crop Loss from Ozone, J. Air Pollut. Control Assoc., 32(4), 353–361, doi:10.1080/00022470.1982.10465408, 1982.

Helmig, D., Lang, E. K., Bariteau, L., Boylan, P., Fairall, C. W., Ganzeveld, L., Hare, J. E., Hueber, J. and Pallandt, M.: Atmosphere-ocean ozone fluxes during the TexAQS 2006, STRATUS 2006, GOMECC 2007, GasEx 2008, and AMMA 2008 cruises, J. Geophys. Res. Atmos., 117(4), 1–15, doi:10.1029/2011JD015955, 2012.

Högström, U.: Non-dimensional wind and temperature profiles in the atmospheric surface layer: A re-evaluation, Boundary-Layer Meteorol., 42(1–2), 55–78, doi:10.1007/BF00119875, 1988.

Johnson, P. N. and Davis, R. A.: Diffusivity of ozone in water, J. Chem. Eng. Data, 41(6), 1485–1487, doi:10.1021/je9602125, 1996.

Kaimal, J. C., Wyngaard, J. C., Izumi, Y. and Coté, O. R.: Spectral characteristics of surface-layer turbulence, Q. J. R. Meteorol. Soc., 98(417), 563–589, doi:10.1002/qj.49709841707, 1972.

Kawa, S. R. and Pearson, R.: Ozone budgets from the dynamics and chemistry of marine stratocumulus experiment, J. Geophys. Res., 94(D7), 9809, doi:10.1029/jd094id07p09809, 1989.

Kirby, S., Dobosy, R., Williamson, D. and Dumas, E.: An aircraft-based data analysis method for discerning individual fluxes in a heterogeneous agricultural landscape, Agric. For. Meteorol., 148(3), 481–489,

doi:10.1016/j.agrformet.2007.10.011, 2008.

Kljun, N., Calanca, P., Rotach, M. W. and Schmid, H. P.: A simple two-dimensional parameterisation for Flux Footprint Prediction (FFP), Geosci. Model Dev., 8(11), 3695–3713, doi:10.5194/gmd-8-3695-2015, 2015.

Langford, B., Acton, W., Ammann, C., Valach, A. and Nemitz, E.: Eddy-covariance data with low signal-to-noise ratio: Time-lag determination, uncertainties and limit of detection, Atmos. Meas. Tech., 8(10), 4197–4213, doi:10.5194/amt-8-4197-2015, 2015.

Lelieveld, J. and Dentener, F. J.: What controls tropospheric ozone?, J. Geophys. Res., 105(1999), 3531, doi:10.1029/1999JD901011, 2000.

Lenschow, D. H. and Kristensen, L.: Uncorrelated noise in turbulence measurements, J. Atmos. Ocean. Technol., 2(1), 68–81, doi:10.1175/1520-0426(1985)002<0068:UNITM>2.0.CO;2, 1985.

Lenschow, D. H., Pearson, R. and Stankov, B. B.: Measurements of ozone vertical flux to ocean and forest, J. Geophys. Res. Ocean., 87(C11), 8833–8837, doi:10.1029/JC087iC11p08833, 1982.

Luhar, A. K., Galbally, I. E., Woodhouse, M. T. and Thatcher, M.: An improved parameterisation of ozone dry deposition to the ocean and its impact in a global climate-chemistry model, Atmos. Chem. Phys., 17(5), 3749–3767, doi:10.5194/acp-17-3749-2017, 2017.

Luhar, A. K., Woodhouse, M. T. and Galbally, I. E.: A revised global ozone dry deposition estimate based on a new two-layer parameterisation for air-sea exchange and the multi-year MACC composition reanalysis, Atmos. Chem. Phys., 18(6), 4329–4348, doi:10.5194/acp-18-4329-2018, 2018.

Macdonald, S. M., Gómez Martín, J. C., Chance, R., Warriner, S., Saiz-Lopez, A., Carpenter, L. J. and Plane, J. M. C.: A laboratory characterisation of inorganic iodine emissions from the sea surface: Dependence on oceanic variables and parameterisation for global modelling, Atmos. Chem. Phys., 14(11), 5841–5852, doi:10.5194/acp-14-5841-2014, 2014.

Magi, L., Schweitzer, F., Pallares, C., Cherif, S., Mirabel, P. and George, C.: Investigation of the Uptake Rate of Ozone and Methyl Hydroperoxide by Water Surfaces, J. Phys. Chem. A, 101(27), 4943–4949, doi:10.1021/jp970646m, 1997.

Mammarella, I., Kolari, P., Rinne, J., Keronen, P., Pumpanen, J. and Vesala, T.: Determining the contribution of vertical advection to the net ecosystem exchange at Hyytiäläforest, Finland, Tellus, Ser. B Chem. Phys. Meteorol., 59(5), 900–909, doi:10.1111/j.1600-0889.2007.00306.x, 2007.

Martino, M., Mills, G. P., Woeltjen, J. and Liss, P. S.: A new source of volatile organoiodine compounds in surface seawater, Geophys. Res. Lett., 36(1), 2–6, doi:10.1029/2008GL036334, 2009.

Martino, M., Lézé, B., Baker, A. R. and Liss, P. S.: Chemical controls on ozone deposition to water, Geophys. Res. Lett., 39(5), 39–43, doi:10.1029/2011GL050282, 2012.

Massicotte, P., Asmala, E., Stedmon, C. and Markager, S.: Global distribution of dissolved organic matter along the aquatic continuum: Across rivers, lakes and oceans, Sci. Total Environ., 609, 180–191, doi:10.1016/j.scitotenv.2017.07.076, 2017.

McKay, W. A., Stephens, B. A. and Dollard, G. J.: Laboratory Measurements of Ozone Deposition To Sea-Water and Other Saline Solutions, Atmos. Environ. Part a-General Top., 26(17), 3105–3110, 1992.

McVeigh, P., O'Dowd, C. and Berresheim, H.: Eddy Correlation Measurements of Ozone Fluxes over Coastal Waters West of Ireland, Adv. Meteorol., 2010, 1–7, doi:10.1155/2010/754941, 2010.

Medina-Ramón, M., Zanobetti, A. and Schwartz, J.: The effect of ozone and PM10 on hospital admissions for pneumonia and chronic obstructive pulmonary disease: A national multicity study, Am. J. Epidemiol., 163(6), 579–588, doi:10.1093/aje/kwj078, 2006.

Metzger, S.: Surface-atmosphere exchange in a box: Making the control volume a suitable representation for in-situ observations, Agric. For. Meteorol., 255(December 2017), 68–80, doi:10.1016/j.agrformet.2017.08.037, 2018.

Metzger, S., Durden, D., Sturtevant, C., Luo, H., Pingintha-Durden, N., Sachs, T., Serafimovich, A., Hartmann, J., Li, J., Xu, K. and Desai, A. R.: Eddy4R 0.2.0: A DevOps model for community-extensible processing and analysis of eddy-covariance data based on R, Git, Docker, and HDF5, Geosci. Model Dev., 10(9), 3189–3206, doi:10.5194/gmd-10-3189-2017, 2017.

Moreno, C. and Baeza-Romero, M. T.: A kinetic model for ozone uptake by solutions and aqueous particles containing I − and Br − , including seawater and sea-salt aerosol , Phys. Chem. Chem. Phys., 19, doi:10.1039/c9cp03430g, 2019.

Morris, J. C.: The aqueous solubility of ozone - a review, Ozone News, 1, 14–16 [online] Available from: http://bmt-berlin.com/Lit-1_CMorris.pdf, 1988.

Pacyna, J. M.: Atmospheric Deposition, in Encyclopedia of Ecology, Five-Volume Set, pp. 275–285., 2008.

Pound, R., Sherwen, T., Helmig, D., Carpenter, L. and Evans, M.: Influences of oceanic ozone deposition on tropospheric photochemistry, Atmos. Chem. Phys. Discuss., 1–25, doi:10.5194/acp-2019-1043, 2019.

Ross, A. N. and Grant, E. R.: A new continuous planar fit method for calculating fluxes in complex, forested terrain, Atmos. Sci. Lett., 16(4), 445–452, doi:10.1002/asl.580, 2015.

Sarwar, G., Kang, D., Foley, K., Schwede, D., Gantt, B. and Mathur, R.: Technical note: Examining ozone deposition over seawater, Atmos. Environ., 141, 255–262, doi:10.1016/j.atmosenv.2016.06.072, 2016.

Shaw, M. D. and Carpenter, L. J.: Modification of ozone deposition and I2 emissions at the air-aqueous interface by dissolved organic carbon of marine origin, Environ. Sci. Technol., 47(19), 10947–10954, doi:10.1021/es4011459, 2013.

Sherwen, T., Chance, R. J., Tinel, L., Ellis, D., Evans, M. J. and Carpenter, L. J.: A machine learning based global sea-surface iodide distribution, Earth Syst. Sci. Data Discuss., (March), 1–40, doi:10.5194/essd-2019-40, 2019.

Smayda, T. J.: Patterns of variability characterizing marine phytoplankton, with examples from Narragansett Bay, ICES J. Mar. Sci., 55(4), 562–573, doi:10.1006/jmsc.1998.0385, 1998.

Squires, F. A., Nemitz, E., Langford, B., Wild, O., Drysdale, W. S., Acton, W. J. F., Fu, P., Grimmond, C. S. B., Hamilton, J. F., Hewitt, C. N., Hollaway, M., Kotthaus, S., Lee, J., Metzger, S., Pingintha-durden, N., Shaw, M., Vaughan, A. R., Wang, X., Wu, R., Zhang, Q. and Zhang, Y.: Measurements of traffic dominated pollutant emissions in a Chinese megacity, Atmos. Chem. Phys. Discuss., (x), 1–33, 2020.

Starkenburg, D., Metzger, S., Fochesatto, G. J., Alfieri, J. G., Gens, R., Prakash, A. and Cristóbal, J.: Assessment of despiking methods for turbulence data in micrometeorology, J. Atmos. Ocean. Technol., 33(9), 2001–2013, doi:10.1175/JTECH-D-15-0154.1, 2016.

Stevenson, D. S., Young, P. J., Naik, V., Lamarque, J. F., Shindell, D. T., Voulgarakis, A., Skeie, R. B., Dalsoren, S. B., Myhre, G., Berntsen, T. K., Folberth, G. A., Rumbold, S. T., Collins, W. J., MacKenzie, I. A., Doherty, R. M., Zeng, G., Van Noije, T. P. C., Strunk, A., Bergmann, D., Cameron-Smith, P., Plummer, D. A., Strode, S. A., Horowitz, L., Lee, Y. H., Szopa, S., Sudo, K., Nagashima, T., Josse, B., Cionni, I., Righi, M., Eyring, V., Conley, A., Bowman, K. W., Wild, O. and Archibald, A.: Tropospheric ozone changes, radiative forcing and attribution to emissions in the Atmospheric Chemistry and Climate Model Intercomparison Project (ACCMIP), Atmos. Chem. Phys., 13(6), 3063–3085, doi:10.5194/acp-13-3063-2013, 2013.

Vaughan, A. R., Lee, J. D., Shaw, M. D., Misztal, P. K., Metzger, S., Vieno, M., Davison, B., Karl, T. G., Carpenter, L. J., Lewis, A. C., Purvis, R. M., Goldstein, A. H. and Hewitt, C. N.: VOC emission rates over London and South East England obtained by airborne eddy covariance, Faraday Discuss., 200, 599–620, doi:10.1039/c7fd00002b, 2017.

Vickers, D. and Mahrt, L.: Evaluation of the air-sea bulk formula and sea-surface temperature variability from observations, J. Geophys. Res. Ocean., 111(5), doi:10.1029/2005JC003323, 2006.

Webb, E. K., Pearman, G. I. and Leuning, R.: Correction of flux measurements for density effects due to heat and water vapour transfer, Q. J. R. Meteorol. Soc., 106, 85–100 [online] Available from: http://www3.interscience.wiley.com/journal/114056302/abstract, 1980.

Wesely, M. L. and Hicks, B. B.: A review of the current status of knowledge on dry deposition, Atmos. Environ., 34(12–14), 2261–2282, doi:10.1016/S1352-2310(99)00467-7, 2000.

Whitehead, J. D., Mcfiggans, G. B., Gallagher, M. W. and Flynn, M. J.: Direct linkage between tidally driven coastal ozone deposition fluxes, particle emission fluxes, and subsequent CCN formation, Geophys. Res. Lett., 36(4), 1–5, doi:10.1029/2008GL035969, 2009.

Wienhold, F.: Micrometeorological measurement and source region analysis of nitrous oxide fluxes from an agricultural soil, Atmos. Environ., 29(17), 2219–2227, doi:10.1016/1352-2310(95)00165-U, 1995.

Wilczak, James, M., Oncley, Steven, P. and Stage, Steven, A.: Sonic anemometer tilt correction algorithms, Boundary-Layer Meteorol., 99(1), 127–150, doi:10.1023/a:1018966204465, 2001.

World Meteorological Organisation: Guide to meteorological instruments and methods of observation., 7th ed., WMO-No. 8., 2008.

Xu, K., Metzger, S. and Desai, A. R.: Surface-atmosphere exchange in a box: Space-time resolved storage and net vertical fluxes from tower-based eddy covariance, Agric. For. Meteorol., 255(October 2017), 81–91, doi:10.1016/j.agrformet.2017.10.011, 2018.

Yang, M., Bell, T. G., Hopkins, F. E., Kitidis, V., Cazenave, P. W., Nightingale, P. D., Yelland, M. J., Pascal, R. W., Prytherch, J., Brooks, I. M. and Smyth, T. J.: Air-sea fluxes of CO2 and CH4 from the penlee point atmospheric observatory on the south-west coast of the UK, Atmos. Chem. Phys., 16(9), 5745–5761, doi:10.5194/acp-16-5745-2016, 2016a.

Yang, M., Bell, T. G., Hopkins, F. E. and Smyth, T. J.: Attribution of atmospheric sulfur dioxide over the English Channel to dimethyl sulfide and changing ship emissions, Atmos. Chem. Phys., 16(8), 4771–4783, doi:10.5194/acp-16-4771-2016,

2016b.

Yang, M., Bell, T. G., Brown, I. J., Fishwick, J. R., Kitidis, V., Nightingale, P. D., Rees, A. P. and Smyth, T. J.: Insights from year-long measurements of air-water CH4 and CO2 exchange in a coastal environment, Biogeosciences Discuss., 16, 961–978, doi:10.5194/bg-2018-503, 2019a.

Yang, M., Norris, S. J., Bell, T. G. and Brooks, I. M.: Sea spray fluxes from the southwest coast of the United Kingdom-Dependence on wind speed and wave height, Atmos. Chem. Phys., 19(24), 15271–15284, doi:10.5194/acp-19-15271-2019, 2019b.

Yuan, R., Kang, M., Park, S. Bin, Hong, J., Lee, D. and Kim, J.: Expansion of the planar-fit method to estimate flux over complex terrain, Meteorol. Atmos. Phys., 110(3), 123–133, doi:10.1007/s00703-010-0113-9, 2011.

Zhou, X. and Mopper, K.: Photochemical production of low-molecular-weight carbonyl compounds in seawater and surface microlayer and their air-sea exchange, Mar. Chem., 56(3–4), 201–213, doi:10.1016/S0304-4203(96)00076-X, 1997.

Table 1: Selection criteria applied to calculated fluxes, with number (and percent) of points remaining.

Selection Criterion	Number of 20-minute periods (%)
Sufficient data in 180–240° wind sector	723 (100%)
Ozone stationarity (trend < 6 ppbv)	689 (95.3%)
Wind stationarity (σ_{wd}) < 10°	655~~30~~ (~~87.1~~90.6%)
Ozone variability σ_{O3} < 2 ppbv	~~55~~609 (~~77.3~~84.2%)
Sensitivity within 3σ of mean	~~54~~710 (~~75.7~~98.2%)
Wind speed > 3 m s^{-1}	~~491~~ 584 (~~67.9~~80.8%)
All of the above	491 (67.9%)

Formatted Table

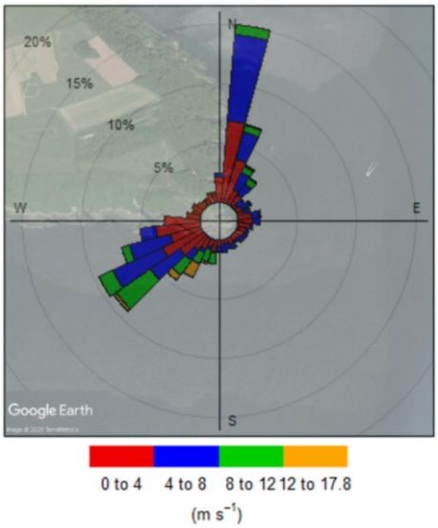

Figure 1: Wind directions and speeds at the PPAO during the study period. Radial percentage values indicate the portion of all observed wind that fell within a given sector. Winds are strong and frequent from the direction of interest in the south-west. © Google Earth.

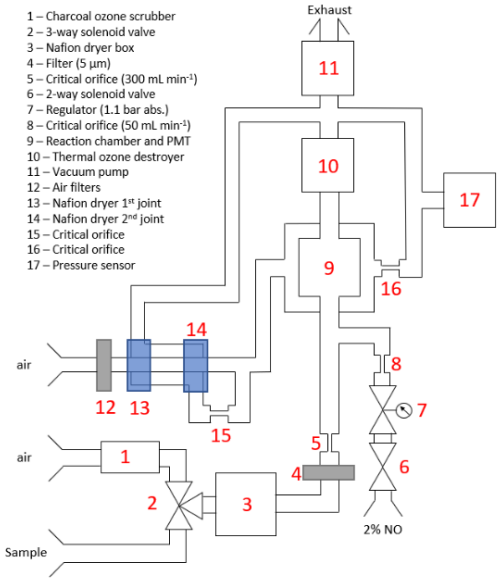

Figure 2: Schematic of the ozone chemiluminescence detector.

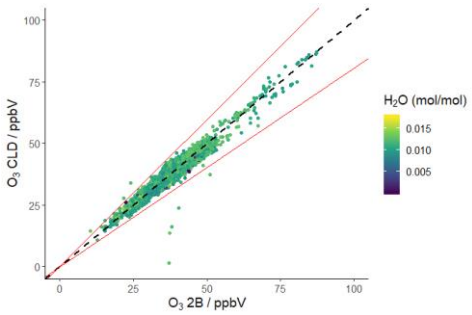

~~**Figure 3: Comparison of 2B and CLD measured ozone concentration using a fixed sensitivity for the CLD of 240 counts ppbv^{-1} s^{-1}. The dotted line is x = y, and the red lines indicate a 3σ deviation from mean sensitivity, used in data filtering. Colour bar indicates the water vapour mixing ratio.**~~

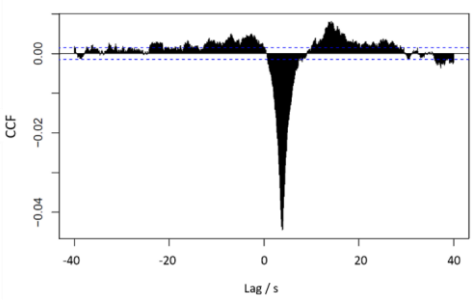

Figure 34: Example cross correlation function (CCF) for ozone and vertical wind on 10th April. The negative peak minimum indicates that ozone data lags 3.9 seconds behind the wind data.

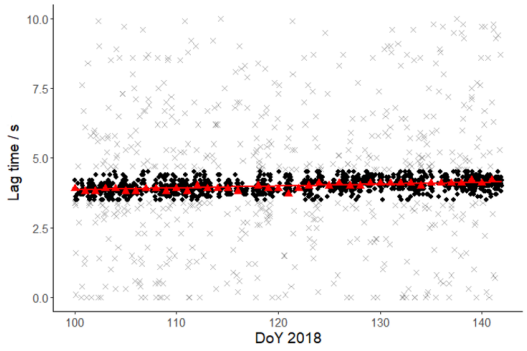

~~**Figure 5: Lag times determined for each 20-minute period. Lags between 3.5 and 4.5 seconds (black dots) were accepted and used to plot a linear fit (red line). Determined lags outside of these bounds (grey crosses) were rejected, and were instead set to the linear fit. Lags determined from daily CCF are shown as red triangles.**~~

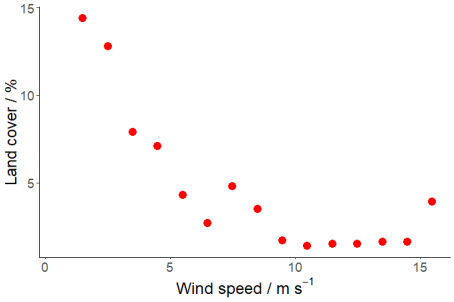

Figure 46: Land cover percentage within the average flux footprint for 1 m s⁻¹ wind speed bins as calculated with the Kljun et al. (2015) flux footprint ~~model~~parameterisation. The presence of land within the footprint area was greater during periods of low wind speed and atmospheric instability

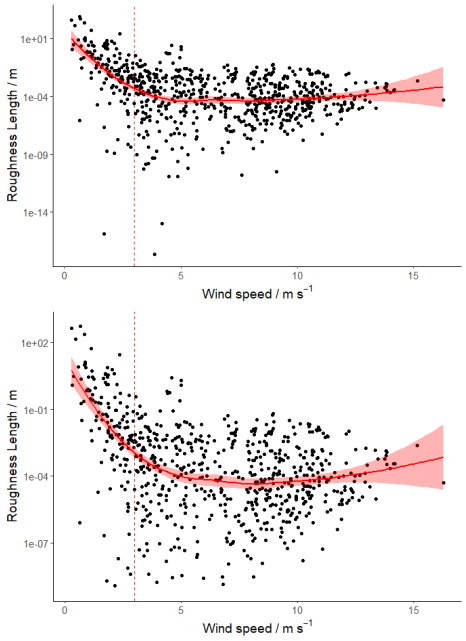

820

Figure ~~7~~5: Roughness length for each averaging period, increased by land influence within the footprint at low wind speeds, with a smoothed line of fit (solid red). ~~and~~Points left of the 3 m s⁻¹ filter threshold (dashed red) are not used in subsequent discussions of oceanic deposition velocity. Y axis limited for clarity, with 17 points < 10⁻⁹ m not shown.

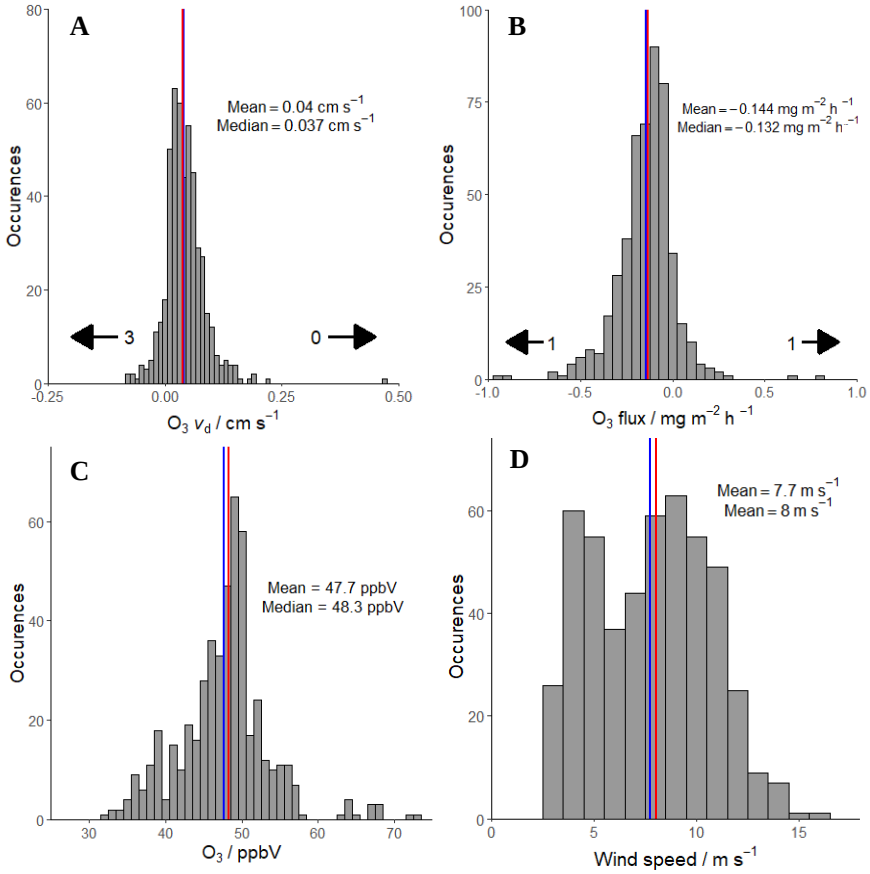
A
Mean = 0.04 cm s−1
Median = 0.037 cm s−1
3
0
Occurences
O3 vd / cm s−1
B
Mean = −0.144 mg m−2 h−1
Median = −0.132 mg m−2 h−1
1
1
Occurences
O3 flux / mg m−2 h−1
C
Mean = 47.7 ppbV
Median = 48.3 ppbV
Occurences
O3 / ppbV
D
Mean = 7.7 m s−1
Mean = 8 m s−1
Occurences
Wind speed / m s−1

825

Figure 68: Ozone deposition velocity (A), mass flux (B), ozone concentration (C) and wind speed (D) histograms for all periods that passed the filtering criteria. Mean values are represented by blue lines, median values by red lines. Deposition velocity and mass flux are plotted in the range -0.25 – 0.50 cm s^{-1} and -1.0 – 1.0 mg m^{-2} h^{-1} respectively for clarity, with arrows indicating the number of points beyond these limits.

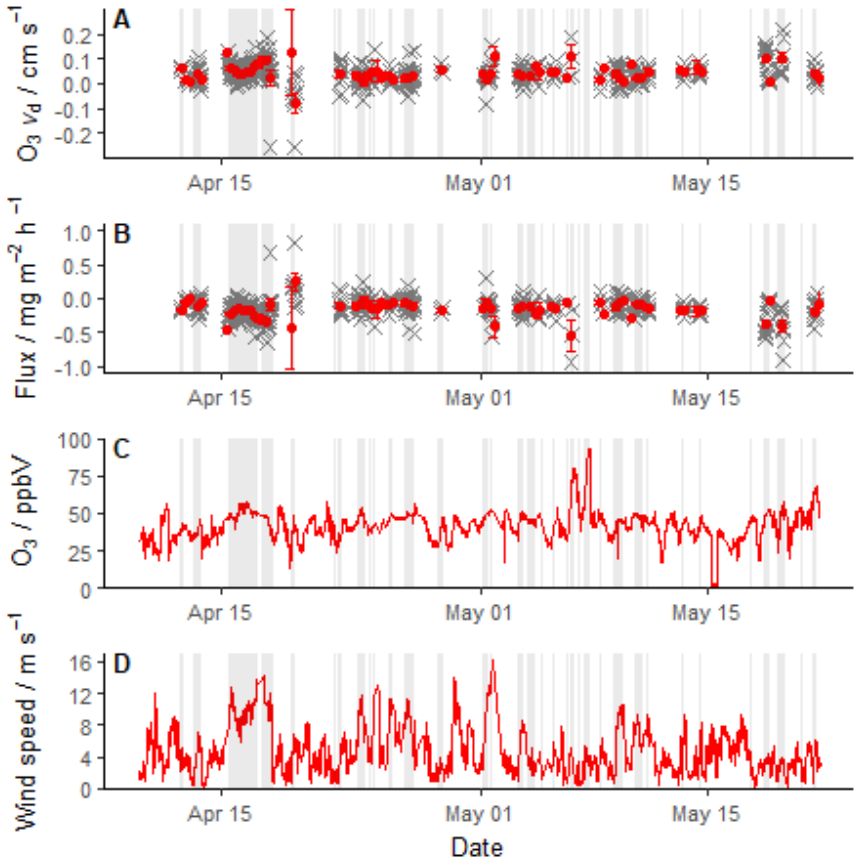

Figure 79: Time series of ozone deposition velocity (A), ozone mass flux (B), mean ozone concentration (C) and mean wind speed (D) from 10th April to 21st May 2018. Grey crosses represent 20-minute values, with red dots for 6-hour means with standard errors. All concentration and wind speed data are shown from 10th April to 21st May, with only deposition/flux values that passed filtering criteria shown in (A) and (B). Periods with an accepted wind direction (180-240°) are shaded. Flux and deposition velocity data are thus only presented from these periods and when the wind speed was > 3 m s^{-1} (D). The y axis in (A) and (B) are limited ~~at~~ to ± 0.3 cm s^{-1} and ± 1 mg m^{-2} h^{-1} respectively

for clarity. Points ~~omitted~~ beyond these y axis bounds are v_d = -0.442 (1.47 mg m^{-2} h^{-1}) and v_d = 0.472 (-1.64 mg m^{-2} h^{-1}), ~~causing~~ which cause the large error bars on April 19th.

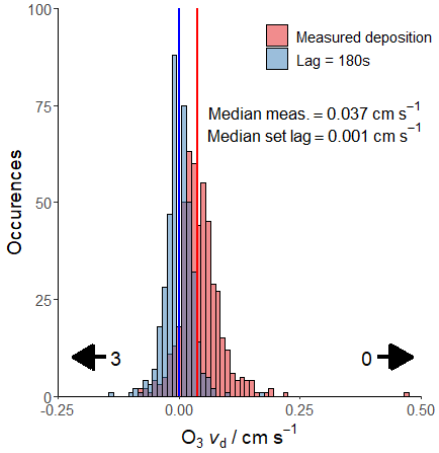

~~**Figure 10: Observed deposition velocity (red) vs deposition observed with lag = 180s (blue). Medians given by respectively coloured lines. X axis limited from -0.25 – 0.5 for clarity, with the number of points out of these bound indicated by the arrows**~~

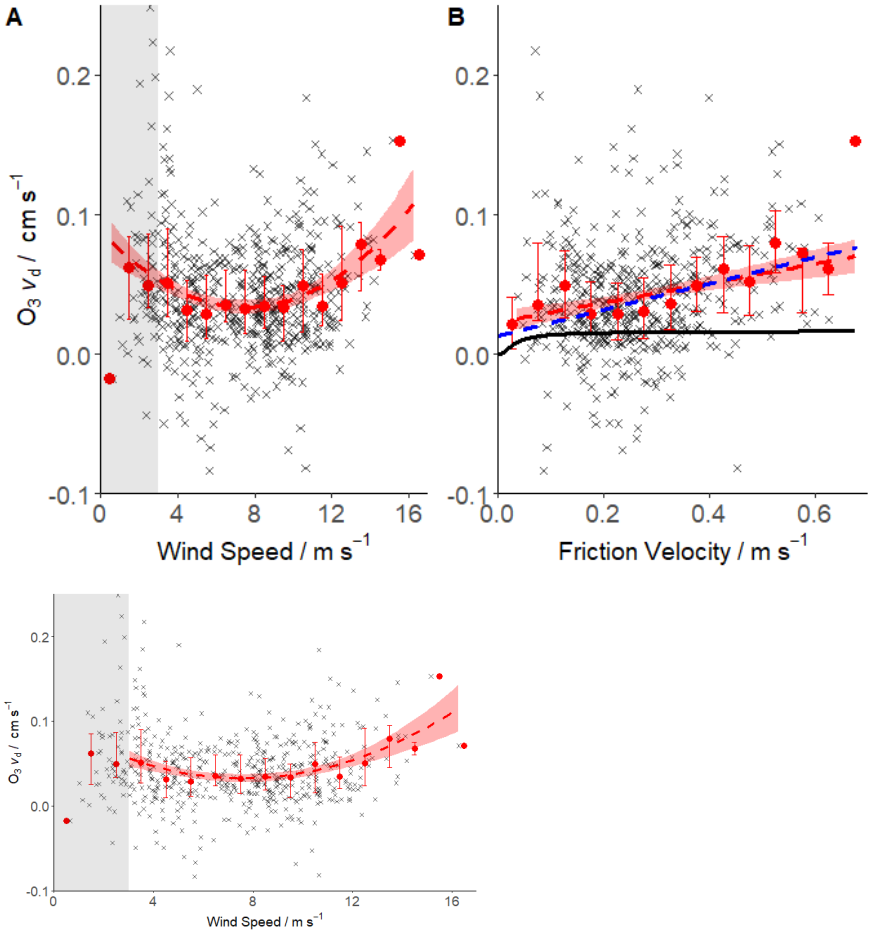

845 **Figure ~~8~~11: Deposition velocity dependence on wind speed ~~(A) and friction velocity (B)~~. 20-minute values are shown in grey, with bin-averaged medians (1 ~~and 0.05~~ m s^{-1} ~~respectively~~) with interquartile ranges shown in red. Wind speed dependence is ~~presented~~ shown with a 2nd order polynomial fit~~,~~ ~~with~~ The grey region below 3 m s^{-1} indicate~~sing~~ values removed by the wind speed filter (Sect. 2.4) that are not included in the fit~~. Friction velocity dependence is presented with a linear fit in red, with the dependence predicted by Fairall et al. (2007) in blue and that predicted by~~**
850 **~~Luhar et al. (2018) in black~~.**

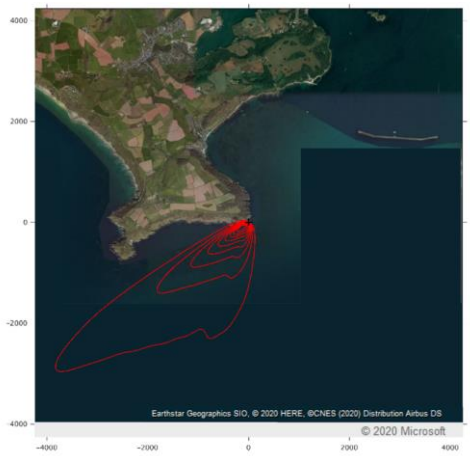

Figure 9~~12~~: Flux footprint climatology for all 20-minute data that passed the selection criteria according to the Kljun et al. (2015) footprint model. Each contour represents the area contributing 10% of the observed flux, up to 90% for the outermost contour. A binary land/sea classification estimated a mean land contribution of 3.9%.

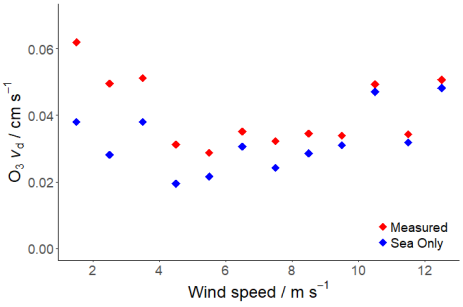

855

Figure 10~~3~~: Median deposition velocities in 1 m s^{-1} wind speed bins for combined land and water surfaces as measured (red) and for water surfaces only (blue). Values at the lowest wind speeds are most influenced by land, and

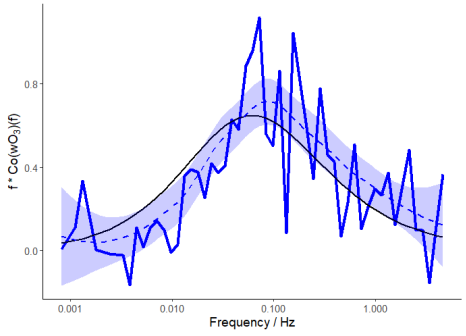

periods with wind speeds below 3 m s^{-1} were not included in the final results.

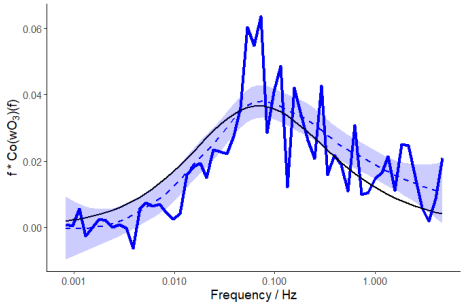

Figure 114**: Average** ~~normalised~~ **ozone flux co-spectrum for the 17th April**, normalised to area = 1**. Wind speeds were 10.3 – 12.3 m s^{-1} and dimensionless Obukhov lengths were 0.14 – 0.17, representing near neutral, slightly stable conditions.** Expected co-spectral shape predicted by (**Kaimal et al. ,(1972)**~~Kaimal prediction~~ **shown in black.** The agreement between observations and Kaimal suggests that the full range of flux-carrying turbulent eddies are being reasonably well measured.

Formatted: Font: Bold
Formatted: Font: Bold
Field Code Changed

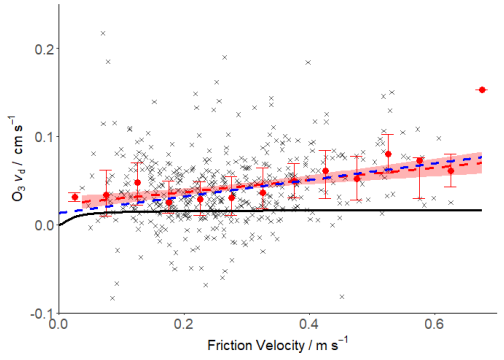

Figure 12: Deposition velocity dependence on friction velocity. 20-minute values are shown in grey, with bin-averaged median fluxes (0.05 m s^{-1} bins) with interquartile ranges shown in red. Dependence of O_3 deposition velocity on friction velocity is presented with a linear fit in red, with the dependence predicted by Fairall et al. (2007) in blue, and that predicted by Luhar et al. (2018) in black.

Formatted: Font: 10 pt, Bold
Formatted: Font: 10 pt, Bold
Formatted: Font: 10 pt, Bold
Formatted: Font: 10 pt, Bold

Response to Referees' Comments

Below we present each original comment (black), followed by the response given in our author comments (red) and what changes were made (blue). Line numbers given in blue refer to the document with track changes displayed. Referee comments will have their original line numbers, corresponding to the original submission.

Referee 1

This paper describes coastal ozone flux measurements made at a location on the south coast of the UK. The paper builds on previous techniques to process & understand the data including its uncertainty. The paper includes a comparison of the data to estimates from oceanic ozone deposition models. The way that the paper is written most benefits readers who are very familiar with oceanic ozone deposition measurements and models. I would urge the authors to make changes in order to expand the readership. One way of doing so would be to better characterize what they are doing (and why) before the results of a given analysis are presented. There are also a lot of figures and information to take in – is this necessary?

We have made efforts to broaden the audience for the article. The one- and two-layer models are now described thoroughly in the introductory section, and the behaviour of these models with respect to wind speed / friction velocity is mentioned as context for the discussion later in the paper. A description of the resistance model for deposition velocities is also included for some background. While we feel the figures presented are informative, some are less dependent on being presented alongside the text. As such what were Figures 3, 5, and 10 have been moved into a supplementary information document to accompany the paper.

L78-118: Descriptions of resistance and deposition models added.

Figures 3, 5 and 10 moved to supplementary information (as Figures S1, S2 and S3)

My only major concern has to do with the footprint analysis, a large component of the paper. The footprint model used is for flat homogeneous terrain rather than heterogenous coastal site. I understand that a footprint model for the given land type may not be available, but I think the authors should explain more, with references, how a footprint model for a flat homogeneous terrain may or may not capture the footprint of a heterogeneous coastal site.

We have expanded the discussion of footprint limitations in line 333 as follows:

It is worth reiterating that this footprint model is designed for use in homogenous environments, which is not true of our site. Furthermore, the double rotation applied to the wind data will result in varying pitch angles relative to the water surface, introducing a dependence of the footprint extent on this pitch angle. These limitations may be important for work relying on direct interpretations of the flux footprint, such as comparisons to emissions inventories (Squires et al., 2020; Vaughan et al., 2017). In contrast to this kind of inventory comparison, we use aggregate footprints, made from several of these individual footprints, only to develop a strategy for robust data selection. This approach follows the works of Amiro (1998), Göckede et al. (2006, 2008); Kirby et al. (2008), Metzger (2018) and Xu et al. (2018) who have demonstrated the utility of aggregation for deriving robust footprint-based metrics in heterogeneous environments.

L378-386: Sentence above expanded

Abstract:

Does the percentage of the flux footprint being water change with tide, or the size of footprint?

The percentage of the footprint being over land will vary some as the tide goes in and out, though it's true the major effects are from changes in wind and stability. We have qualified that footprint size has an effect as well in the abstract.

L21-24: Include footprint variation on stability, and by extension footprint extent.

Readers may not know the Fairall model well. Can the authors add some short description of this model to the abstract instead of, or in addition to, referring to the reference?

A brief description of the Fairall model has been included in the abstract

L27-31: Description of Fairall model added, along with the Luhar model and its description.

Can the authors clarify whether they are talking about fluxes or deposition velocities when they refer to 'deposition'? (this applies throughout the paper and the figures; I tend to think that 'deposition' refers to the flux')

'Deposition' has been specified to 'deposition velocity' or flux as appropriate throughout the document.

'Deposition' has been amended as above in all instances.

Line 26 – I think this a rather strong statement; only one paper suggests this

Altered the statement to convey that 25% is just an estimate, and the true value may be lower.

L39-40: Added 'as much as'. Also added more references in agreement (Ganzeveld, Pound).

Line 31– briefly describe what is meant by 'atmospheric and surface resistance values'

Definitions for both atmospheric and surface resistance have been added in parentheses.

L46-52: Added equation of resistance in series, with definitions.

L56: description of surface resistance in parentheses.

Line 31 – rephrase so as not to imply that we can't learn anything from these lab and box enclosure methods

This sentence has been reworded to properly convey the value of box-enclosure experiments in determining surface resistance values

L55: 'Such experiments are valuable in determining…'

Line 36 – references for this range of values? are the citations given in the previous sentences just for seawater?

All eddy covariance measurements referenced were over saltwater. We have qualified that the range of values given corresponds specifically to the eddy covariance measurements referenced in the prior sentence.

L61-62: ‘The deposition velocities reported in the few eddy covariance observations over saltwater…’

Line 52 – clarify the aspect of the depositional sink that needs to be better characterized, in line with the discussion in the previous paragraph; also, is it really a ‘tropospheric ozone cycle’?

We have specified that it is the effects of wind speed and of the composition of the sea surface that are in need of better characterisation. The term ‘cycle’ was not appropriate – this has been changed to ‘budget’.

L119-120: ‘Better characterisation of the effects of wind speed and sea-surface composition on ozone deposition velocity to the sea surface would significantly improve our understanding of the global tropospheric O_3 budget’

Line 55 – not sure this is the right usage of the term ‘natural variability’

Removed ‘natural’ instead encompassing more generally ‘factors’ that could affect uncertainty in the measurements

L123-124: ‘Factors affecting the variation…’

Line 74 – can the authors describe more clearly in the text what Figure 2 shows and what the author wants the reader to do in referring to all the parts

The ‘parts’ had been intended to aid conveniently in referring to Figure 2. However, we realise this may be redundant given the presence of these labels within the figure. These ‘part’ labels have been removed from the body of text, but left in Figure 2.

L142-148: Part numbers removed for clarity.

Line 105 – check sentence Line

Sentence completed – corrections not needed ‘for determining an accurate ozone mixing ratio’.

L181: Sentence completed as above.

112 – what is ‘dry ozone’?

Reworded to convey ‘in the absence of water vapour’

L189: ‘…supply of ozone in the absence of water vapour...’

Line 130 – there is a negative sign missing

Minus sign added, and rearranged for Flux on the left-hand side.

L44: Equation 1 corrected, and rearranged for flux on the left-hand side.

Line 148-149 – what is ‘contrary’? are the authors implying that the dependences of Chang and Helmig are incorrect?

The opposite is intended – rather the dependencies of Chang and Helmig cause us to be wary of our data at low wind speeds. The sentence has been reworded, qualifying that we observe an 'apparent increase' in deposition velocity at low wind speed, most likely from land interference rather than genuinely higher deposition over the water.

L259-263: Sentences reworded as follow: 'Additionally, higher deposition velocities were observed during periods of very low winds, contrasting with the trend of increasing deposition velocity with wind speed proposed by Chang et al. (2004) and observed during open ocean cruises by Helmig et al. (2012). Yang et al. (2016, 2019) observed a similar enhancement in CO_2 transfer at low wind speeds, and chose to filter out low wind speed data'

Line 150 – new paragraph starting at "Footprint analysis"

Separated into a new paragraph as requested

L227: 'Flux footprint analysis' starts a new paragraph

Line 159 – where is this estimate of roughness length from? is it appropriate for the location?

Eq. (12) is a rearrangement of the logarithmic wind profile equation to solve for roughness length (this has been added to the text for clarity). Due to the lack of roughness elements over the sea, the displacement height term has been omitted.

L238-239: Mention the use of measured values and the logarithmic wind profile

Line 170 –removal 'of'

'off' corrected to 'of'

L257: Typo amended

Line 171 – clarify this sentence; what is the object of "contributing"?

Clarified 'contributing to the elevated surface roughness values'

L258-259: 'Roughness' added

Line 171-4 – can the authors clarify what they are doing here? are they further filtering their data based on the roughness lengths or not? if not, is the justification only that they don't want excessive data removal?

We confirm that roughness length has not been used as a filtering parameter – we merely note it as a potential alternative. Figure 5 shows that a roughness length filter of approximately $z_0 < 0.1$m would only really exclude points already removed by the wind speed filter. Lowering that threshold would begin to remove several points across the full range of wind speeds, and we wish to retain as many points as possible for when data are later separated further into wind speed bins.

L263-264: We clarify that the wind filter is used wherever medians are reported for the whole data set.
L265-266: Removed sentence to avoid ambiguity.

Line 175-180 – but does it mean anything for the authors' conclusions with regards to wind speed or friction velocity dependencies?

This criterion was in fact 0.10 m s^{-1}, not 0.15 m s^{-1} as stated. This has been corrected. A threshold of 0.15 m s^{-1} only makes a tiny difference too though: 0.001 cm s^{-1}.

This small difference is because the wind speed filter already applied removed the vast majority of very low u_* values, since they scale approximately linearly with each other over the ocean. The additional u_* filter made little difference (only removing 30 points), having little effect of the median given the number of data points clustered around that median. Giving values to 4 decimals would show the 0.10 m s^{-1} u_* filter would increase the median deposition from 0.00371 cm s^{-1} to 0.00373 cm s^{-1}, but a change of less than 1% cannot be considered significant here.

To avoid confusion, we have clarified that we are discussion a u_* filter in addition to the previously applied criteria, rather than as a substitute for wind speed.

L271: 0.15 m s^{-1} corrected to 0.1 m s^{-1} for considered friction velocity filter
L271-272: Qualified that this was considered in addition to previous filter criteria

Line 183 – what is being compared with the 20-min averaging?

60-minute averaging – added for clarity

L276: Added 'when using 60-minute averaging'

Line 186 – "Flux and deposition velocity values"

'Deposition' added

L301: 'velocity' added to subheading

Line 189-191 – say what this finding means

The Kolmogorov-Smirnov test shows that our distribution of values and the distribution where wind and ozone data are disjoined could not have been picked at random from the same distribution of values. Therefore, we are observing a flux that is statistically distinct from the noise in the measurements. A sentence has been added to clarify this.

L306-308: Added 'This confirms that the experimental set-up used here has a sufficiently low limit of detection to discern the flux from noise over the whole duration of the measurements'

Line 193-4 –say what this finding means

Clarified that the average flux value obtained was above the 2σ LoD, but with considerable uncertainty associated with it.

L309-311: 'This confirms that the experimental set-up used here has a sufficiently low limit of detection to discern the flux from noise over the whole duration of the measurements'

Line 220 – is there a reference for this equation?

This equation comes from the assumption that atmospheric surface stress and waterside surface stress are equal. This is the assumption made by Luhar et al. (2017), and the reference has been added.

L503-504: Note section discussing wind speed dependence moved to discussion. Added: 'with u_{*w} derived from u_* assuming atmospheric surface stress to be equal to the waterside surface stress (Luhar et al., 2017)'

Line 229 – is an assumption of constant Ts and [I-] fair? what's the 'relevant' time periods?

'relevant period' changed to 'April-May' to clarify that we are using the model values that span the period of the observations. SST and I are certain to vary, and to affect reactivity – the iodide especially will be the subject of future work where we quantitatively measure iodide (and other species) concentrations in the microlayer within the footprint area. However since a detailed set of these data were not yet available for this publication, the sources of data used by Luhar et al. have been used here as well for consistency.

L515: Specified April-May, and the source of iodide data

Line 232 & 234 – what are the confidence intervals for m + b?

Standard errors have been added for the gradient and intercept of the linear fit of our deposition velocities against u_*. Similar values for the Fairall model are not readily available – they are not quoted when these values are given in the work of Helmig et al. (2012), and assessing the uncertainties in the original model are beyond the scope of this work.

L520: Standard error values added to the linear fit.

Line 237 – in terms of 'remarkable' I recommend the authors remain objective

Language changed to be more objective.

L524:526: Wording changed: 'Given the assumptions of the simplified model (Eq. (20)) and the uncertainties in various parameters, not least the rate constant for the reaction of O_3 with I^- (e.g. Moreno & Baeza-Romero, 2019), this agreement is perhaps surprising'

Line 239 – why consider only iodide reactivity? and I'm not actually sure what this means – I thought the authors were fixing [I-]. Does this mean that the authors are only considering the temperature dependence of A? generally, it would help if the authors gave brief descriptions of the Fairall and Luhar models, otherwise the discussion is not very useful for readers who are not well versed in oceanic ozone dep models. the authors do this to some degree in the discussion, but it would be nice to have this information closer to the beginning of the article.

A sentence has been added to clarify that 'only iodide reactivity' is meant to convey that we are not attempting to add a quantitative reactivity term for organic material (as mentioned in section 4) or anything else. This means the model fits are for a single reactivity and temperature, and therefore a single A value, to examine wind speed / u_* dependence while other conditions are fixed at values typical for our site.
Regarding the models, a sectioning introducing both models, their assumptions and dependencies has been added to the introduction to properly cover this ahead of the discussion.

L527: Added '(i.e. omitting any enhancement in reaction rate due to the presence of organic material in both models)'
L78-118: Section introducing deposition models added early in the manuscript.

Line 240 – while the Luhar model underpredicts vd, it doesn't seem like the variability in the Luhar model is necessarily off, or worse than Fairall. Can the authors provide quantitative metrics for how well these models fit the data?

Root mean square error (RMSE) and mean bias values have been added for both models. RMSE is high in both cases due to the large scatter in the data, but it is smaller for the Fairall parameterisation than for the 2-layer model. Mean bias is small for the Fairall parameterisation, and much larger for the two-layer model.

L522-524: Metrics for Fairall: 'Comparison of our data to this parameterisation yielded a root mean square error (RMSE) of 0.0522 cm $^{-1}$ and a mean bias of 0.0020 cm s^{-1} (a positive bias here denoting observations greater than the model)'
L529-530: Metrics for Luhar model: 'Comparison of our data to the two-layer model gave higher RMSE and mean bias (0.0584 cm s^{-1} and 0.0247 cm s^{-1} respectively)'

Line 244 – what is the object of amplifying?

Amplifying the potential influence 'of land deposition' - added for clarity

L364: 'amplifying the potential influence of land deposition on our data'

Line 245 – is this deposition velocity for grassland from the models used in Hardacre et al.? or some observations used in the Hardacre model evaluation? regardless, the authors need to clarify and discuss the high uncertainty in using this value, and use references for the observations at grasslands if they are using the observations. Generally, I'm not sure what we are learning from the analysis with the Hardacre grassland value.

The deposition velocity estimate is taken from the medians of the two datasets analysed by Hardacre et al. (2015), specifically Figures 4c and 4d. The inclusion of this quick calculation is intended to serve as a demonstration of how much on an influence land could potentially have on a coastal measurement if land exists within the flux footprint. This is then followed with an attempt at determining a more realistic value for our site given the land is not true 'grassland'. We have also qualified that the value we use is a median of the accumulated datasets used by Hardacre et al. (2015).

L365-366: Specified median of Hardacre data used: 'median land deposition value from datasets analysed by Hardacre et al., (2015)'

Line 251 – confidence intervals for the land and sea values?

Standard errors for the regression of land % with deposition added

L372-373: '…yielded values of 0.167 $\pm$ 0.080 cm s^{-1} and 0.034 $\pm$ 0.016 cm s^{-1} for land and sea respectively'

Line 259 – I don't follow why ozone fluxes would be compared to emission inventories

Reference is made to inventories to highlight the kind of studies where more precise footprint areas are essential for lining up with sources. This is included to contrast with our work where the footprint is used more for quality control rather than trying to match up to specific sources and sinks.

L382-383: Text adjusted: 'In contrast to an inventory comparison, we only use the flux footprint model to develop a strategy for robust data selection, and generate an aggregate footprint from several individual footprints'

Line 260 – in contrast to what? what do the authors mean by 'aggregates'?

Clarified 'contrast to this kind of inventory comparison' – aggregate refers to an 'average' of individual, 20-minutely footprints. 'made from several of these individual footprints' added to clarify this.

L382: 'In contrast to an inventory comparison…'
L383: '…from several individual footprints'

Line 263 – why is this example 'extreme'? perhaps best to remain objective

We would maintain that this example is extreme, but realise we neglected to explain why – the tidal zone was very shallow in the work of Whitehead et al. (2009), meaning that at low tide the flux footprint was almost entirely over ~3 km of exposed seabed rather than water. These details have been added to justify the 'extreme'.

L391-392: given details of why the example is extreme: 'This large variation in their work was a consequence of a 9 m tidal range exposing the sea floor up to 3 km from the shore'

Line 265 – what could this mean in terms of the results? generally it might be better to have all the info about the tides in one paragraph, not two, with some of the info tacked on the end of a very long paragraph

The estuarine input to the coastal waters could change the chemical composition of the surface water, and thus its reactivity to ozone. Chemical analysis of the surface water does not form a part of this manuscript however, and will be a focus of our future work. A sentence has been added to clarify this. Additionally, 'Tidal influence' has been separated into its own subchapter, with both paragraphs merged within to distinguish it clearly from the prior section.

L387: New subsection for tidal discussion
L393-394: 'This altered composition could affect the reactivity of ozone at the sea surface. Such effects will be examined in future work'

Line 266 – measurement height was adjusted how/where?

Clarified that we are referring to the measurement height used in flux and footprint calculations. The physical tower height was not changed, but the height of the tower above the water varied with tide, and this was the 'adjustment' made to the mean height above sea level to properly account for this change in footprints etc.

L426: reworded to 'Tower height above the water was determined for all flux calculations using'

Line 270 – where the authors expecting to see a diurnal cycle? would be helpful if authors set the stage for describing this analysis more

Added that a diurnal was not expected – we merely provide the information given its presence in the discussion of Gallagher et al. (2001). The lack of a diurnal cycle also suggests land deposition to be minimal.

L432-434: 'However, no diurnal variability was observed in the PPAO O_3 flux data (as might be expected due to deposition to land), again implying minimal land influence in our filtered observations.'

Line 273 – describe method of Langford briefly

The following sentence provides a brief description of the method. We feel a more in depth description would feel out of place here. The initial presentation of this and the theoretical flux uncertainty calculation methods are now introduced in section 2.5.

L279-299: Error methods introduced earlier as section 2.5 in Materials and Methods

Line 285 – in what relationship?

Clarified that we refer to the relationship in equation 16.

L289-290: 'A factor with a value of 1–2 is sometimes also included **in the numerator of Eq. (16)** to reflect uncertainty in this relationship'

Line 294 – similar to what literature? include references

Specified that we mean values for near-neutral conditions – references of Blomquist et al (2010) and Lenschow and Kristensen (1985) provided.

L429: two references for *b* value added

Line 295 – meaning that the authors do not use equation12 to calculate the integral timescale?

Equations (now updated) 17 and 18 are used with the peak of the co-spectrum in Figure 11 to determine our *a* value. This *b* value is then used in equation 18 using the wind and height data for each 20-minute period to estimate an integral timescale for each period.

Added that equations 17 and 18 are used with Figure 11 to determine the *b* value for clarity.

L428: 'Using Eq. (17) and Eq. (18), this corresponds…'

Line 299 – repeat empirical value here

Value added

L435: 'compared with the empirical value of 0.113 mg m^{-2} h^{-1}'

Line 301– what do the authors mean 'they defined twice'?

Bad wording – clarified to 'right-hand side of Eq. (16) multiplied by 2'.

L289-290: Reworded again to 'A factor with a value of 1–2 is sometimes also included in the numerator of Eq. (16)…'

Line 302 – clarify here that talking about variability within the averaging interval

'within averaging intervals' added as requested.

L438: 'Equation (16) demonstrates how the variability of ozone and vertical wind within averaging intervals are…'

Line 303-4 – this sentence confuses me. random instrument noise in the ozone measurement or the wind measurement?

This was poorly phrased – it has been changed to specify that noise is the ozone instrument is likely a large part of ozone variance.

L440-441: ‘random noise in the ozone instrument likely represents a significant contribution to the total variance of ozone observed at 10 Hz’

Line 319 – say what the results with respect to block averaging vs. linear detrending means

Added a clause explaining that the use of linear detrending is not leading to large low-frequency information loss.

L457: ‘…implying that linear detrending is not causing much low frequency information loss’

Line 324 – give the percentage for random uncertainty here

Percentage (85%) added, as well as clarification that this is a 2σ uncertainty.

L460-461: ‘…a small amount relative to the calculated 2σ random uncertainty (85%)’

Line 329 – does this choice of reaction-diffusion sublayer length have an impact on results? where is this estimate from?

It was erroneously stated in the original text that a fixed sublayer depth was used in this model estimate. That approach was investigated, but it is the variable length, parameterised from diffusivity and reactivity (the equation for which is now given as Eq. (11)) in the amended introduction) that was ultimately used. The script has been corrected to reflect this. For interest, the use of a fixed 3 µm layer rather than the variable layer (which works out as 4.2 µm) leads to a model estimate of 0.018 cm s^{-1}, up from 0.016 cm s^{-1}. This is a relatively small change in depth, given the range of 1.2 – 24 µm for waters varying 2-33 °C in temperature.

L111: Added equation used to parameterise sublayer depth
L470: sublayer depth corrected to 4.2, reference to Equation 11

Line 333-4 – cut ‘significantly’

‘Significantly’ removed

L474: ‘…is likely to be higher…’

Line 353-5 – I’m confused by these sentences; rephrase

Reworded to reflect that the two-layer model gives values more similar in magnitude to our observations, but gives a wind speed dependence fundamentally different from some observed data.

L533-536: ‘The two-layer model is set up to account for ozone reactions with chemical species other than iodide. Inclusion of these additional reactions would increase the predicted deposition velocity to be more similar to our observations. However, the two-layer model also predicts that v_d does not strongly depend upon variations in wind speed, which is in contrast with our observations.’

Line 360 – why just discuss Helmig values here?

Comparison to previous values determined from tower-based eddy covariance measurements added (McVeigh, Whitehead).

L541-542: added McVeigh and Whitehead values and references.

Line 376 – give numbers here for instrument noise uncertainty

Limit of detection (0.113 mg m^{-2} h^{-1}) and noise level contribution to ozone variation (45-98%) added.

L545: median LoD value added
L546-547: Noise percentage added

Line 378-9 – clarify what the authors mean by larger (longer or additional measurements or both?)

We intended for both – changed to reflect this – 'A longer dataset with more chemical composition variables'

L573-574: 'A longer time series with more observations of microlayer chemical composition may help…'

Table 1 – say whether the data in the nth row is filtered by the criteria in the previous n-1 rows

Altered the table as per Reviewer 3's suggestion for each row to show only that filter from the total, with a row at the bottom showing the application of all values.

L796: Table filters done individually, with a total at the bottom

Figure 4 – it's so helpful here that the authors point out what the reader should be "getting" from this figure – can the authors do this for other figures?

Figure 1, 3, 7, 10, 12, 13, and 14 captions amended to clarify the 'take-away' message from the figure. As mentioned, Figures 3 and 10 are now moved to SI, now Figures S1 and S3 respectively.

L800 onwards: figure captions above updated

Figure 5 – say what 'DoY' is

Plot x axis label changed to 'Day of Year 2018' (and moved to SI, Figure S2).

Figure moved to SI, DoY changed to 'Day of Year 2018'

Figure 9 – instead of saying "points omitted" (which to me implies that the authors do not include the data in the averages), can the authors say something like "points outside the y axis range"?

'omitted' changed to 'beyond these y axis bounds'. Note, renumbered to Figure 7

L837: 'Points beyond these y axis bounds'

Figure 12 – I don't know what I'm supposed to be looking at here/what this figure is telling me

The footprint plot is included to give an idea of the spatial area being observed over the course of these measurements. We realise the previous caption was unhelpful for anyone not familiar with contoured footprint plots, and as such has been updated to describe the bounds represented. Note, renumbered to Figure 9

L852-853: 'Each contour represents the area contributing 10% of the observed flux, up to 90% for the outermost contour.'

Figure 14 – ‘kaimal prediction’ is not very clear

Changed to ‘Expected cospectral shape predicted by Kaimal…’ to better explain its use as an ‘expected’ reference point. Note, renumbered to Figure 11

L862: ‘Expected co-spectral shape…’

Referee 2

Linear detrending is often followed by time-tapering, e.g., by a Hamming window. Was this done?

Time tapering has not been used in this work – instantaneous fluctuations have been determined directly from the linear trend of each averaging period.

No change has been made for this comment

For fixed tower sites, a planar fit (Wilczak et al) or some other triple-rotation method is often used. Perhaps this should be investigated, particularly because it could be an issue for small fluxes.

Early in the data processing, the effect of using planar fit method in place of double rotation was investigated. A general planar fit method with one set of rotation co-ordinates is clearly inappropriate for our site on a headland. A sector planar fit (10°) however agreed well with the double rotation method. Given the small difference (~4%) in fluxes, we chose to pursue double rotation, and avoid the disjoint in tilt angles experienced by a sector planar fit approach.

A small section detailing this train of thought has now been included in the paper where the double rotation application is discussed.

L172-179: Added brief discussion of rotation methods and their consequences

Suggest figure 7 be rescaled with a lower limit of at least 10ˆ-9. Two or three very small outliers are compressing the real data.

Figure 7 (now Figure 5) has been rescaled to a lower limit of 10^{-9} m as suggested. The caption has also been updated to acknowledge the points beyond this boundary.

L819: Y axis rescaled on Figure 5

Referee 3

L57. I would name this chapter as 2. Materials and Methods. And then having subchapters 2.1 Measurement location; 2.2. Experimental setup; 2.3 Flux calculation.2.4. Data selection; etc.

A ‘Materials and Methods’ chapter has been made as suggested, with subheadings ‘Measurement location’, ‘Experimental set-up’, ‘Pre-flux processing’, ‘Data selection’ and ‘Flux uncertainty’.

L126: Experimental section title changed to 'Materials and Methods'. Consists of: Measurement location, Experimental set-up, Pre-flux processing, Data selection and a newly added section Flux uncertainty (to introduce these methods earlier).

L104-105. There is something missing at the end of the sentence. Please check it.

Sentence completed – corrections not needed 'for determining an accurate ozone mixing ratio'.

L181: Sentence finished - '…were unnecessary for determining an accurate ozone mixing ratio'

L114-127. Why to use such large windows for searching the lag, e.g. from 0 to 10sec as shown in Fig.4? I would use a very narrow window (e.g. 4±1) sec in order to reduce the scatter.

The large lag window is somewhat arbitrary, but if a clear peak cannot be identified above the noise is such a large timespan, then limiting the window to, say, 2-6 seconds will just result in a random peak in the noise being chosen (closer to the 'true' lag). We would prefer to set the lag time to a good estimate in such cases where no clear peak is observed, hence the large bounds. Note this is now Figure 3.

We have not changed our lag calculation window, arguing that if a clear covariance peak is not present using a small lag window, a large window will still result in a 'noise peak' being chosen. We would prefer to set the lag using our linear fit in this case, rather than have a peak picked within our lag bounds (3.5 – 4.5 seconds) by chance that may not be the true lag.

L130. A minus sign is missing from Eq.1.

Minus sign added, and rearranged putting flux on the left-hand side.

L44: Equation 1 corrected, and rearranged for flux on the left-hand side.

L140 - Please report the percentage of excluded data for each criteria, and also the total percentage of data left.

Table 1 amended for each row to show only the effect of each filter on the total data set. A row at the bottom has then been added showing the combined effect of all filters on the data (with percentages provided in all cases).

L796: Table filters done individually, with a total at the bottom

L156-157. Why? I do not understand this point. Footprint doesn't depend on windspeed, rather on stability. I would be interested to see footprint estimates for different stability classes. Did the authors use the estimated roughness length for the footprint calculation?

The roughness length used in footprint determination was that calculated by Eqs. (12-15). Depending on the chosen scaling approach, footprint parameterizations are expressed as a combination of variables that interrelate the strengths of horizontal and vertical transport processes. These can include atmospheric stability (but don't have to, e.g,. Kljun et al., 2004) and horizontal wind speed (e.g., Kormann and Meixner, 2001). Subject to similar solar forcing and owing to the differing albedo and heat capacity of the water surface, the diurnal cycle of stability is less pronounced in the coastal boundary layer compared to the boundary layer over land. On the other hand, subject to similar horizontal pressure gradient and owing to differing roughness, the resulting horizontal wind speed over the water surface is greater compared to over the land surface. Resulting from these processes underlying the coastal boundary layer, we chose the horizontal wind speed over atmospheric stability to provide the more selective

discriminator for water and land surfaces, and classifier for footprint extent. Figures 4 and 5 demonstrate the robustness of this approach.
A clearer list of all variables used in the footprint calculation has also been added.

References:
Kljun, N., Calanca, P., Rotach, M. W., and Schmid, H. P.: A simple parameterisation for flux footprint predictions, Boundary Layer Meteorol., 112, 503-523, doi:10.1023/B:BOUN.0000030653.71031.96, 2004.
Kormann, R., and Meixner, F. X.: An analytical footprint model for non-neutral stratification, Boundary Layer Meteorol., 99, 207-224, doi:10.1023/A:1018991015119, 2001.

L230-232: Clarified the rest of the inputs of the footprint parameterisation - 'These were defined using tide-adjusted measurement height, roughness length, friction velocity, wind speed (and direction), crosswind variability, and stability conditions, then aggregated into 1 m s^{-1} wind speed bins'

L172-174. It is not clear when and where this filter based on wind speed was applied. For example, in Figures 9, 11 and 13 data points with U<3 m/s are shown. Please clarify it.

We have clarified (lines 263-264) that the filter is applied wherever overall medians are presented for the dataset or the models.

All filters are applied to flux and deposition velocity values presented in Figure 9 (now 7). Wind speeds below 3 m s^{-1} are shown in 7D to provide a complete timeseries. However, we have now clarified in the caption that there are no corresponding flux or deposition velocity values for these periods due to the filtering.

Figure 11 (now 8) include these points to show the elevation at low wind speeds graphically. The omission of these points from the final dataset is made clear in the caption, with a shaded region indicating the removed region of values.

Figure 13 (now 10) similarly deals with exploring the unwanted influence of land, and these low wind speed values are therefore instrumental in doing this. We have added another clarification in this caption that the values below the wind speed threshold were removed from final flux and deposition velocity values.

L263:264: 'A wind speed filter of > 3 m s^{-1} was used in this work where median fluxes and deposition velocities are reported for the whole dataset (or model work)'

L835-836: Clarified the wind data presence in figure Caption - 'Flux and deposition velocity data are thus only presented from these periods and when the wind speed was > 3 m s^{-1} (D)'

5.4 Measurement uncertainty. Most of this section describe the approaches to calculate the flux random uncertainty, and then it should be moved under the Materials and Methods chapter.

Descriptions of both the empirical and theoretical methods for uncertainty calculation have been moved into their own subsection of the Materials and methods Section. Discussion of their application to the data have been left in results so that presented values of uncertainty can be considered comparatively with the flux and deposition velocity values presented in the preceding section.

L279: Flux uncertainty section added as section 2.5 under Materials and Methods, introducing both error methods ahead of their application.

L280. For the estimation of total random uncertainty note also the Finkelstein and Sims (2001) method, which do not require the estimate of the integral timescale (which may be not so straightforward). See Rannik et al (2016) for a comprehensive review of existing approaches.

We recognise the work of Finkelstein and Sims (2001) as an alternative method for estimating flux variance, and note its use of covariance functions similarly to that of Langford et al. (2015) presented in this work. While not included in this manuscript, its implementation as an alternative method in the eddy4R workflow will be considered in the continuation of these measurements.

We have not added another error calculation method in this work, owing to its similarity to that of the Langford method.

L284. What do the authors mean by "integral timescale for vertical fluctuations? "This should be the integral timescale of instantaneous covariance timeseries w'X' (see Rannik et al, 2016)

This wording was ambiguous, and has been changed as suggested for clarity

L289: Corrected – '…is the integral timescale for the instantaneous covariance time series *w'X''*

L316-317. What about the response time of the O3 analyser and the sensor separation? Could the authors provide more details?

The sample inlet was position approximately 20 cm below the anemometer – this has been added to the text. Although a precise value has not been accurately recorded in the field, lab tests determined the response time to be < 1 second, and the co-spectrum (Fig. 11) does not indicate high-frequency flux loss to be very large.

L514-515: Added – 'Sensor separation was minimised by locating the sample inlet directly beneath the sonic anemometer (~20 cm below)'

Figure 14. It is not clear for me how the cospectrum was normalized. Values seems to be one order of magnitude lower than what should be the reference Kaimal cospectrum. Units in the figure axis labels could be put between parenthesis.

An error was made in the initial normalisation – the plot has been updated to correctly assign the area beneath the data to be equal to 1 (now figure 11).

L923: Figure 11 updated with corrected normalisation

Other

Other minor corrections (typos, etc) have been made, as well moving the discussion of the dependence of deposition velocity on wind speed to the discussion section (rather than results).

Formatted: Font color: Accent 1, Check spelling and